Systematic approach to β and $2\nu\beta\beta$ decays of mass $A = 100$–136 nuclei

Pekka Pirinen and Jouni Suhonen
University of Jyväskylä, Department of Physics, Post Office Box 35 (YFL), FI-40014, Finland
(Received 16 January 2015; revised manuscript received 10 April 2015; published 11 May 2015)

In this work we perform a systematic study of pairs of single-β-decaying nuclei in the mass region $A = 100$–136 to extract information on the effective value of the axial-vector coupling constant g_A. As the many-body framework we use the quasiparticle random-phase approximation (QRPA) and its proton-neutron variant (pnQRPA) in single-particle valence bases with Woods-Saxon-calculated single-particle energies. It is found that, to a reasonable approximation, g_A is a linear function of the mass number A, with a slightly different parametrization below and above the mass $A = 121$. Using the values of g_A extracted from the linear fit, as well as an average constant value of g_A, we calculate the two-neutrino double-β ($2\nu\beta\beta$) decay half-lives of 11 $\beta^-\beta^-$ decays and 10 mixed β^+ and electron-capture (EC) decays, $\beta^+\beta^+/\beta^+$EC/ECEC, to both the ground state and the lowest three excited states.

DOI: 10.1103/PhysRevC.91.054309 PACS number(s): 21.60.Jz, 23.40.Bw, 23.40.Hc, 27.60.+j

I. INTRODUCTION

The research on double-β decay is both timely and of great interest for particle and nuclear physics [1–3]. Both the neutrinoless double-β ($0\nu\beta\beta$) and two-neutrino double-β ($2\nu\beta\beta$) decays depend sensitively on the involved nuclear matrix elements (NMEs). A large number of different nuclear models have been used to describe the associated nuclear wave functions. Among these models are the quasiparticle random-phase approximation (QRPA), its proton-neutron extension (pnQRPA) (see Ref. [4] and references therein), and its renormalized extensions [5,6]. A different category of nuclear models are formed by the interacting shell model (ISM) [7], the (proton-neutron) interacting boson model (IBA-2) [8], the Gogny-based energy-density functional approach (EDF) [9], and the projected Hartree-Fock-Bogoliubov mean-field scheme (PHFB) [10]. An extensive comparison of the double-β properties of the aforementioned models is performed in Ref. [11].

The $2\nu\beta\beta$ decays can occur in two different categories: The decays on the β^- side, i.e., $2\nu\beta^-$ decays, have favorable decay Q values and abundances, and they have been under intensive experimental and theoretical investigation over the years. Many decay transitions have already been detected for these decays [12]. The positron-emitting modes of decays, $2\nu\beta^+\beta^+$, $2\nu\beta^+$EC, and 2νECEC (generically called $2\nu\beta^+/$EC hereafter, EC referring to electron capture) are much less studied due to their relatively low Q values and abundances. No such decay transitions have yet been observed in the laboratory. On the theory side, these decays have been investigated for their lepton aspects in Ref. [13] and nuclear-structure aspects, e.g., in Refs. [14–22]. Some of these studies refer to decays to the ground states and some refer to decays to both ground and excited states.

The phase space of the $2\nu\beta^-$ and $2\nu\beta^+/$EC decays depends on the fourth power of the value of the weak axial-vector coupling constant g_A. Hence, it is of paramount importance to know the (effective) value of g_A in medium-mass and heavy-mass nuclear systems. An effective value of $g_A \sim 1$ has been advocated in several ISM calculations in the past (see, e.g., Refs. [23,24]). Even stronger quenchings have been proposed in Refs. [25,26]. At the same time the pnQRPA, used in the calculations of the involved NMEs, suffers from the "g_{pp} problem," i.e., from the unsettled value of the particle-particle interaction parameter g_{pp} describing the strength of the proton-neutron interaction in the 1^+ channel. Since the introduction of this parameter [27,28], several researchers have tried to fix its values by the inspection of the measured single-β-decay rates [29,30] or $2\nu\beta\beta$ decay rates [31–34].

The effective value of g_A can also be studied together with the value of g_{pp} within the pnQRPA framework. The first work on this line of study is that of Ref. [35] where both the β-decay and $2\nu\beta^-$-decay data were analyzed for the $A = 100,116$ systems in the framework of the pnQRPA using least squares to achieve best-fit values for g_A. In Ref. [35] the best-fit values $g_A = 0.74$ ($A = 100$) and $g_A = 0.84$ ($A = 116$) were obtained. A monotonic behavior of g_A as a function of the mass number A was parametrized in Ref. [36] by analyzing the magnitudes of the NMEs of several $2\nu\beta^-$ decays computed by the IBA-2 model. In this study the obtained g_A-versus-A slope was very flat. Simultaneous use of the $2\nu\beta^-$ and β^- data for the $A = 100,116,128$ systems lead to a much quenched value of $g_A \sim 0.6$ in Refs. [37,38]. In Ref. [39] the interacting boson-fermion-fermion model (IBFFM-2) was used to derive effective value of $g_A \sim 0.3$ in the $A = 128$ case. In Ref. [40] an extension of the g_A analysis to first-forbidden $2^- \to 0^+_{gs}$ β decays was achieved.

In the present article we adopt a more systematic approach to attack the problem of the effective value of g_A. We are going to allow the values of both g_A and g_{pp} to vary in an analysis of 24 isobaric triplets within the mass range $A = 100$–136. In these triplets an intermediate odd-odd isobar connects via β transitions to its two adjacent even-even isobars and the rates of the connecting transitions are experimentally known. We try to reproduce the measured transition rates in a pnQRPA calculation by varying g_A and g_{pp} in each isobaric triplet separately. In this way the present analysis is an extension of that of Ref. [41] where nine such pairs were analyzed within a very rudimentary pnQRPA approach. At the same time the present study extends the idea of Ref. [40], i.e., of using the geometric mean of the decay rates, to the Gamow-Teller β decays. The geometric means of the two

 ©2015 American Physical Society

decay branches are more stable against variations in g_{pp} and g_A than the individual branches of decay and are thus preferable in the analysis. By this analysis we derive a piecewise linear relationship between the mass number A and the parameter g_A. By using this relationship we then predict $2\nu\beta^-$ and $2\nu\beta^+$/EC decay half-lives for a total of 21 nuclei in the mass range $A = 100$–136. We also compare these predictions with those derived from a constant mean value of g_A.

This article is organized as follows: In Sec. II we give a brief introduction to the underlying formalism of the Gamow-Teller β transitions, and the $2\nu\beta^-$ and $2\nu\beta^+$/EC decays. In Sec. III we display and discuss the obtained single-β-decay and double-β-decay results. The final conclusions are drawn in Sec. IV.

II. REVIEW OF THE FORMALISM OF COMPUTATION

In this section only the basic theoretical ingredients of the computations are given. The single- and double-β decay half-lives are defined in terms of the involved NMEs and the phase-space factors. The NMEs are given in terms of the single-particle matrix elements and the one-body transition densities. For the calculation of the phase-space factors and the one-body transition densities we refer to the available literature at the appropriate places.

A. Gamow-Teller β decays

The Gamow-Teller β-decay transitions are mediated by the Pauli spin operator $\boldsymbol{\sigma}$. In this work we extract the needed experimental Gamow-Teller NMEs by using the experimental comparative half-lives ($\log ft$ values). They are defined as [42]

$$\log ft = \log(f_0 t_{1/2}[s]) = \log\left[\frac{6147}{B_{\rm GT}}\right], \tag{1}$$

where the reduced transition probabilities $B_{\rm GT}$ are given by

$$B_{\rm GT} = \frac{g_A^2}{3}\left|\sum_{pn}\sigma_{pn}(I_f^+\|[c_p^\dagger\tilde{c}_n]_1\|1_1^+)\right|^2, \quad (\beta^-) \tag{2}$$

$$B_{\rm GT} = \frac{g_A^2}{3}\left|\sum_{pn}\sigma_{np}(I_f^+\|[c_n^\dagger\tilde{c}_p]_1\|1_1^+)\right|^2. \quad (\beta^+) \tag{3}$$

The single-particle matrix elements are defined as

$$\sigma_{pn} = \tfrac{1}{3}(p\|\boldsymbol{\sigma}\|n), \quad \sigma_{np} = \tfrac{1}{3}(n\|\boldsymbol{\sigma}\|p), \tag{4}$$

where the matrix elements of the Pauli operator are given in Ref. [42]. In Eqs. (2) and (3) the final states appearing in the one-body transition densities are considered to be $I_f^+ = 0_{\rm gs}^+, 2_1^+, 0_1^+, 2_2^+$, where $0_{\rm gs}^+$ is assumed to be the vacuum state of the quasiparticle random-phase approximation (QRPA), discussed briefly in Sec. II C. The first 2^+ state in the final even-even nucleus, 2_1^+, is considered to be a one-phonon QRPA state and the first excited 0^+ state, 0_1^+, and the second 2^+ state, 2_2^+, are considered to be two-phonon QRPA states; see Sec. II C. Exact expressions for the one-body transition densities are given in Ref. [20].

B. Two-neutrino double-β decays

The two-neutrino double-β decays are of either the $2\nu\beta^-$ or the $2\nu\beta^+$/EC type. The associated half-lives can be expressed as [13,20,43]

$$\left[T_{2\nu}^{\beta^-\beta^-}(I^+)\right]^{-1} = G_{2\nu}^{\beta^-\beta^-}(I^+)\left[M_{2\nu}^{\beta^-\beta^-}(I^+)\right]^2, \tag{5}$$

$$\left[T_{2\nu}^{\beta^+\beta^+}(I^+)\right]^{-1} = G_{2\nu}^{\beta^+\beta^+}(I^+)\left[M_{2\nu}^{\beta^+\beta^+}(I^+)\right]^2, \tag{6}$$

$$\begin{aligned}\left[T_{2\nu}^{\beta^+{\rm EC}}(I^+)\right]^{-1} &= G_{2\nu}^{\beta^+{\rm EC(K)}}(I^+)\left[M_{2\nu}^{\beta^+{\rm EC(K)}}(I^+)\right]^2 \\ &\quad + G_{2\nu}^{\beta^+{\rm EC(L)}}(I^+)\left[M_{2\nu}^{\beta^+{\rm EC(L)}}(I^+)\right]^2,\end{aligned} \tag{7}$$

$$\begin{aligned}\left[T_{2\nu}^{\rm ECEC}(I^+)\right]^{-1} &= G_{2\nu}^{\rm EC(K)EC(K)}(I^+)\left[M_{2\nu}^{\rm EC(K)EC(K)}(I^+)\right]^2 \\ &\quad + G_{2\nu}^{\rm EC(K)EC(L)}(I^+)\left[M_{2\nu}^{\rm EC(K)EC(L)}(I^+)\right]^2,\end{aligned} \tag{8}$$

where the expressions for the lepton phase-space integrals $G_{2\nu}^\alpha(I^+)$, $\alpha = \beta^-\beta^-$ are given in Ref. [1] and the integrals $G_{2\nu}^\alpha(I^+)$, $\alpha = \beta^+\beta^+, \beta^+$EC, ECEC are given in Ref. [13]. The NMEs $M_{2\nu}^\alpha(I^+)$ include energy denominators and a summation over all the 1^+ states of the intermediate nucleus (see below). Above, the symbols EC(K) and EC(L) denote electron captures from the atomic K and L_1 shells, respectively.

The NMEs involved in the above half-life expressions can be cast in the form

$$\begin{aligned}M_{2\nu}^\alpha(I^+) &= \sum_{k_1} M_{k_1}(I^+)F_{k_1}^\alpha(I^+), \\ \alpha &= \beta^-\beta^-, \beta^+\beta^+, \beta^+{\rm EC}, {\rm ECEC},\end{aligned} \tag{9}$$

where in the QRPA framework one writes

$$\begin{aligned}M_{k_1}(I^+) &= \frac{1}{\sqrt{1+2\delta_{I2}}}\sum_{k_2}\sum_{pp'nn'} m(pp',nn') \\ &\quad\times\left(I_f^+\|[c_{p'}^\dagger\tilde{c}_{n'}]_1\|1_{k_1}^+\right)\left\langle 1_{k_1}^+\middle|1_{k_2}^+\right\rangle \\ &\quad\times\left(1_{k_2}^+\|[c_p^\dagger\tilde{c}_n]_1\|0_i^+\right), \quad (2\nu\beta^-)\end{aligned} \tag{10}$$

$$\begin{aligned}M_{k_1}(I^+) &= \frac{1}{\sqrt{1+2\delta_{I2}}}\sum_{k_2}\sum_{pp'nn'} m(nn',pp') \\ &\quad\times\left(I_f^+\|[c_{n'}^\dagger\tilde{c}_{p'}]_1\|1_{k_1}^+\right)\left\langle 1_{k_1}^+\middle|1_{k_2}^+\right\rangle \\ &\quad\times\left(1_{k_2}^+\|[c_n^\dagger\tilde{c}_p]_1\|0_i^+\right). \quad (2\nu\beta^+/{\rm EC})\end{aligned} \tag{11}$$

Here the operator $c_p^\dagger$ ($c_n^\dagger$) creates a proton (neutron) particle in the orbital $p = n_p, l_p, j_p$ ($n = n_n, l_n, j_n$), where n is the radial, l is the orbital angular-momentum, and j is the total single-particle angular-momentum quantum number. The same holds for the particle annihilation operators, written without the dagger. The single-particle parts in Eqs. (10) and (11) are written as

$$m(pp',nn') = \sigma_{p'n'}\sigma_{pn}, \quad m(nn',pp') = \sigma_{n'p'}\sigma_{np}, \tag{12}$$

where the matrix elements of the Pauli operator were defined in Eq. (4).

The one-body transition densities involved in Eqs. (10) and (11) are given separately for the different types of I_f^+ final states in Ref. [20]. Furthermore, the overlap between the

two sets of pnQRPA states used in the calculations is given by

$$\langle J^{\pi}_{k_1}|J^{\pi}_{k_2}\rangle = \sum_{pn}\left[X^{J^{\pi}_{k_2}}_{pn}\bar{X}^{J^{\pi}_{k_1}}_{pn} - Y^{J^{\pi}_{k_2}}_{pn}\bar{Y}^{J^{\pi}_{k_1}}_{pn}\right] \tag{13}$$

and it takes care of the matching of the corresponding states in the two sets of states based on the initial and final even-even reference nuclei. The amplitudes X and Y ($\bar{X}$ and $\bar{Y}$) come from the pnQRPA calculation starting from the initial (final) nucleus of the double-β decay (see Sec. II C). Here it is appropriate to note that the expression (13) is only an approximation if the initial and final ground states are not identical. However, the approximation is reasonable if these ground states are not very different in terms of orbital occupancies.

The quantities $F^{\alpha}_{k_1}(I^+)$ in Eq. (9) are the following energy denominators:

$$F^{\beta^-\beta^-}_k(0^+) = F^{\beta^+\beta^+}_k(0^+) = \left(\Delta_k + \frac{1}{2}W_0\right)^{-1}, \tag{14}$$

$$F^{\beta^-\beta^-}_k(2^+) = F^{\beta^+\beta^+}_k(2^+) = \left(\Delta_k + \frac{1}{2}W_0\right)^{-3}, \tag{15}$$

$$F^{\beta^+\mathrm{EC}}_k(0^+) = \frac{1}{\Delta_k - \varepsilon_{\mathrm{b}1} + \frac{1}{3}W_0^{\beta^+\mathrm{EC}}} + \frac{1}{\Delta_k + \frac{2}{3}W_0^{\beta^+\mathrm{EC}}}, \tag{16}$$

$$F^{\beta^+\mathrm{EC}}_k(2^+) = \frac{\Delta_k + \frac{1}{2}W_0}{\left(\Delta_k - \varepsilon_{\mathrm{b}1} + \frac{1}{3}W_0^{\beta^+\mathrm{EC}}\right)^2\left(\Delta_k + \frac{2}{3}W_0^{\beta^+\mathrm{EC}}\right)^2}, \tag{17}$$

$$F^{\mathrm{ECEC}}_k(0^+) = \frac{1}{\Delta_k - \varepsilon_{\mathrm{b}1} + \frac{1}{2}W_0^{\mathrm{ECEC}}} + \frac{1}{\Delta_k - \varepsilon_{\mathrm{b}2} + \frac{1}{2}W_0^{\mathrm{ECEC}}}, \tag{18}$$

$$F^{\mathrm{ECEC}}_k(2^+) = \frac{\Delta_k + \frac{1}{2}W_0}{\left(\Delta_k - \varepsilon_{\mathrm{b}1} + \frac{1}{2}W_0^{\mathrm{ECEC}}\right)^2\left(\Delta_k - \varepsilon_{\mathrm{b}2} + \frac{1}{2}W_0^{\mathrm{ECEC}}\right)^2}, \tag{19}$$

where the normalized (by the electron rest-mass energy) intermediate energy is given by

$$\Delta_k = (E_k - M_i c^2)/m_e c^2 \tag{20}$$

and the decay energies are

$$\begin{aligned} W_0 &= (M_i c^2 - E_f)/m_e c^2\,; \\ W_0^{\beta^+\mathrm{EC}} &= W_0 + \varepsilon_{\mathrm{b}1}\,, \\ W_0^{\mathrm{ECEC}} &= W_0 + \varepsilon_{\mathrm{b}1} + \varepsilon_{\mathrm{b}2}\,. \end{aligned} \tag{21}$$

Here the quantity E_f is the final-state (ground-state or excited-state) energy and

$$\varepsilon_{\mathrm{b}i} = (m_e c^2 - B_i)/m_e c^2\,, \quad i = 1,2\,, \tag{22}$$

where B_i is the binding energy of electron i in an atomic K or L_1 orbital [13]. In Δ_k [see Ref. (20)] E_k is the energy of the kth 1^+ state in the intermediate nucleus. In the pnQRPA calculations the energy E_k is taken to be the average of the kth energy eigenvalues based on the two pnQRPA calculations, one for the initial and one for the final nucleus of the $\beta\beta$ decay. Furthermore, the energy difference $E_1 - M_i c^2$ is taken from experiment whenever the excitation energy of the first 1^+ state of the intermediate nucleus is known experimentally.

C. Nuclear models

The initial and final 1^+ states of β decays and intermediate 1^+ states of double-β decays (both always in odd-odd nuclei) are handled within the framework of the pnQRPA. The pnQRPA states, in an odd-odd nucleus, can be written as

$$|1^+_k\, M\rangle = \sum_{pn}\left(X^{1^+k}_{pn}[a^\dagger_p a^\dagger_n]_{1M} - Y^{1^+k}_{pn}[a^\dagger_p a^\dagger_n]^\dagger_{1M}\right)|\mathrm{QRPA}\rangle\,, \tag{23}$$

where $|\mathrm{QRPA}\rangle$ is the QRPA vacuum. The operator $a^\dagger_p$ ($a^\dagger_n$) creates a proton (neutron) quasiparticle in the orbital p (n). The sum runs over all proton-neutron configurations in the chosen valence space. In the pnQRPA formalism states (23) connect directly to the neighboring even-even ground states, both in the initial nucleus, $0^+_i = 0^+_{\mathrm{gs}}$, and the final one, $I^+_f = 0^+_{\mathrm{gs}}$.

The wave functions of the final states $I^+_f = 2^+_1, 0^+_1, 2^+_2$ of the β and double-β decays are computed by the use of the multiple-commutator model (MCM) [44,45]. It is designed to connect excited states of an even-even reference nucleus to states of the neighboring odd-odd nucleus. The states of the odd-odd nucleus are given by the pnQRPA in the form (23). The excited states of the even-even nucleus are generated by the (charge conserving) quasiparticle random-phase approximation (QRPA) described in detail in Ref. [42]. Here the symmetrized form of the phonon amplitudes is adopted contrary to Ref. [42] so that the first excited 2^+ state in the final nuclei of the β and double-β decays can be written as a QRPA phonon of the form

$$\begin{aligned} |I^+_f\rangle &= |2^+_1\, M\rangle = Q^\dagger(2^+_1\,, M)|\mathrm{QRPA}\rangle \\ &= \sum_{ab}\left(Z^{2^+_1}_{ab}[a^\dagger_a a^\dagger_b]_{2M} - W^{2^+_1}_{ab}[a^\dagger_a a^\dagger_b]^\dagger_{2M}\right)|\mathrm{QRPA}\rangle\,, \end{aligned} \tag{24}$$

where the amplitudes Z and W are obtained by solving the QRPA equations of motion [42].

From the above 2^+ phonons (24) one can build an ideal two-phonon state of the form

$$|I^+_{2-\mathrm{ph}}\rangle = \frac{1}{\sqrt{2}}[Q^\dagger(2^+_1)Q^\dagger(2^+_1)]_I|\mathrm{QRPA}\rangle\,. \tag{25}$$

An ideal two-phonon state consists of partner states $I^\pi = 0^+, 2^+, 4^+$ that are degenerate in energy, and exactly at an energy twice the excitation energy of the 2^+_1 state. In practice this degeneracy is always lifted by the residual interaction between the one- and two-phonon states [46]. In this work we assume the $I^+_f = 0^+_1$ and $I^+_f = 2^+_2$ final states of β and double-β decays to be reasonably well described by the ansatz wave function (25).

III. RESULTS AND DISCUSSION

In this section we present and discuss the results of the calculations. For the sake of completeness we introduce each of

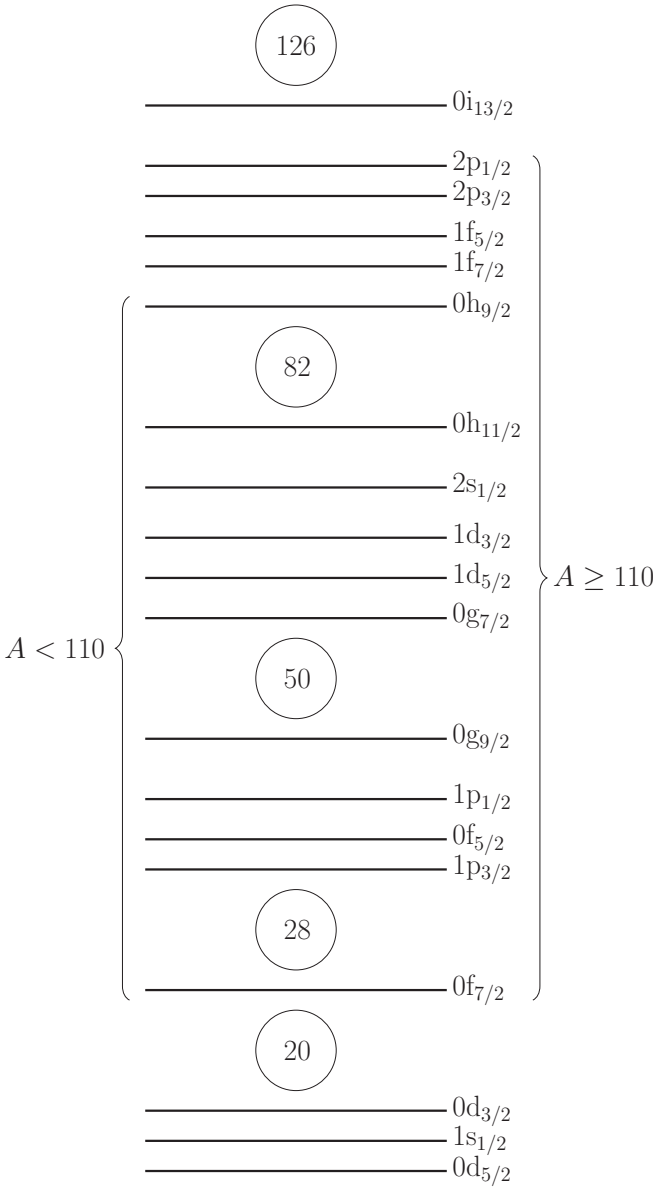

FIG. 1. A schematic figure of the orbitals used to form the bases for nuclei with $A < 110$ and $A \geqslant 110$.

the elements entering the calculations, referring to the already published material for details.

A. Determination of model parameters

Up to $A = 108$ a valence space consisting of 11 states, the entire $1p - 0f - 0g$ and $2s - 1d - 0h$ shells, was used. For $A = 110$ and onwards also the $2p$ and $1f$ shells were included and the valence space was expanded to 15 states. The valence spaces are visualized in Fig. 1. The single-particle bases are built by using a Coulomb-corrected Woods-Saxon potential and solving the radial Schrödinger equation. The Woods-Saxon parameters used were the ones given by Bohr and Mottelson in Ref. [47].

For the two-body part of the interactions, the renormalized Bonn-A G matrix [44,48] has been used and the neutron and proton pairing strength parameters $A^{\mathrm{p}}_{\mathrm{pair}}$ and $A^{\mathrm{n}}_{\mathrm{pair}}$ were fitted such that the lowest quasiparticle energies from the BCS calculation match the pairing gaps:

$$E^{\mathrm{p}}_{\mathrm{qp}}(\mathrm{lowest}) = \Delta_{\mathrm{p}}, \quad \text{and} \quad E^{\mathrm{n}}_{\mathrm{qp}}(\mathrm{lowest}) = \Delta_{\mathrm{n}}.$$

The pairing gaps can be calculated by the three-point formula [49]

$$\begin{aligned}\Delta_{\mathrm{p}}(A,Z) &= \tfrac{1}{4}(-1)^{Z+1}[S_{\mathrm{p}}(A+1,Z+1)\\ &\quad - 2S_{\mathrm{p}}(A,Z) + S_{\mathrm{p}}(A-1,Z-1)],\\ \Delta_{\mathrm{n}}(A,Z) &= \tfrac{1}{4}(-1)^{A-Z+1}[S_{\mathrm{n}}(A+1,Z)\\ &\quad - 2S_{\mathrm{n}}(A,Z) + S_{\mathrm{n}}(A-1,Z)],\end{aligned}$$

where S_{i} is the proton or neutron separation energy. The separation energies were taken from Ref. [50].

The particle-hole and particle-particle interaction strengths are important interaction parameters in both the QRPA and pnQRPA. As a convention for the present work, in the QRPA these parameters are written as uppercase G_{ph} and G_{pp} and in the pnQRPA as lowercase g_{ph} and g_{pp}.

In QRPA, G_{pp} has little effect on the first excited states [51] and the common value of $G_{\mathrm{pp}} = 1.00$ has been adapted for the examined nuclei. The first excited state of the presently studied even-even nuclei is a 2^+ state, which is of a particle-hole nature. Therefore, the value of G_{ph} has a significant effect on the energy of this state. The value of G_{ph} was fixed for each nucleus separately by fitting the energy of the first 2^+ state to experimental data.

In pnQRPA, the particle-hole parameter g_{ph} has a large effect on the energy location of the Gamow-Teller giant resonance (GTGR). The particle-particle parameter g_{pp} has more to do with the Gamow-Teller β-decay transition amplitudes [51]. The value of g_{ph} was fitted for each nucleus separately to approximately match the GTGR location to the empirical formula [42]:

$$\begin{aligned}\Delta E_{\mathrm{GT}} = \Delta E_{\mathrm{C}} + \Delta E_{Z+1,N-1} &= \left[1.444\left(Z+\tfrac{1}{2}\right)A^{-\frac{1}{3}}\right.\\ &\quad \left. - 30.0(N-Z-2)A^{-1} + 5.57\right]\mathrm{MeV}, \qquad (26)\end{aligned}$$

where ΔE_c is the Coulomb energy and $\Delta E_{Z+1,N-1}$ is the energy difference between the GTGR state and the 0^+ isobaric analog state of the odd-odd nucleus.

The particle-particle interaction parameter g_{pp} is often used to fit the log ft value of the transition from the first 1^+ state of the odd-odd nucleus to the ground state of the even-even nucleus [48,51]. In the present work, to better examine the systematics of Gamow-Teller β decay, we assign an array of constant values of $g_{\mathrm{pp}} = 0.6, 0.7, 0.8, 0.9$. By fitting the geometric means of the β-decay matrix elements to experimental values, the behavior of the axial-vector coupling constant g_{A} is expressed as a function of the mass number A for each value of g_{pp}. This enables us to find a systematic behavior of g_{A} for a given value of g_{pp}.

B. Single-β decays and determination of the effective value of g_{A}

In this work a selection of medium heavy nuclei in the mass region $A = 100$–134 are taken under investigation. This

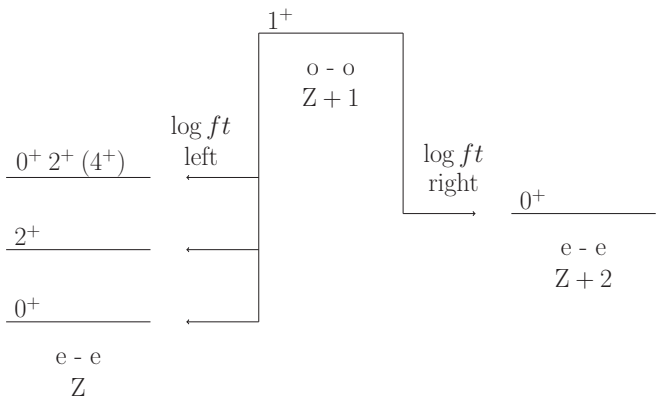

FIG. 2. A schematic of the single-β decay triplets studied in this work. The nucleus in the middle is odd-odd, and its neighbors on the left and right are even-even.

selection spans practically all the nuclei where relevant log ft data have been measured. The nuclei are grouped into triplets where an odd-odd nucleus with a 1^+ ground state is in the "center" and two neighboring even-even isobars with 0^+ ground states are to the "left" and "right" of the odd-odd nucleus as is represented in Fig. 2. Ground-state-to-ground-state β decays as well as decays to excited states of the even-even nuclei are predicted using the QRPA framework.

In the present analysis it is preferable to use the geometric mean of the two transition matrix elements since the geometric mean is practically independent of the value of g_{pp}, as visible in Fig. 3. This owes to the particular behavior of the β^- and β^+/EC decay amplitudes as a function of g_{pp} in a pnQRPA calculation: The β^- (β^+/EC) decay amplitude for a transition from an odd-odd nucleus is a decreasing (increasing) function of g_{pp}, as shown explicitly in Ref. [29]. In this way the g_{pp} dependencies of the two branches conspire to produce an almost flat g_{pp} dependence for the geometric mean.

One can calculate the experimental geometric means of the left and right NMEs (multiplied by g_A) from

$$g_A\mathcal{M}^{m}_{GT}(\text{exp.}) = g_A\sqrt{\left|\mathcal{M}^{l}_{GT}(\text{exp.})\mathcal{M}^{r}_{GT}(\text{exp.})\right|} = \sqrt{6147\times\sqrt{\frac{(2J^l_i+1)(J^r_i+1)}{10^{\log ft_l(\text{exp.})}\times 10^{\log ft_r(\text{exp.})}}}}. \quad (27)$$

This quantity is actually independent of the value of g_A taken for theoretical calculations, which permits g_A to be left as a free parameter to fit calculations to experimental data. The calculated experimental geometric means for the investigated mass region are presented in Table I. The needed experimental log ft values were taken from Ref. [52].

We first examined the ground-state-to-ground-state decays in the investigated mass region. Four rounds of pnQRPA calculations were performed using typical values of $g_{pp} = 0.6, 0.7, 0.8, 0.9$ in order to analyze the left and right branches of Gamow-Teller β decay from each odd-odd nucleus. Theoretical geometric means of these matrix elements were then calculated for each value of g_{pp} and fitted to the experimental values by altering the value of g_A. The calculated matrix elements and geometric means for $g_{pp} = 0.7$ are given in Table II and visualized in Fig. 4. The resulting values of g_A for each value of g_{pp} are presented in Fig. 3 as a function of the mass number A.

In Fig. 4 one can see a decreasing behavior of the NMEs as a function of A. At first, around $A = 100$–112 there is some alternation between the left and right matrix elements being larger than the other, but at $A = 112$ onwards the right matrix elements are always smaller than the left ones and eventually become only about a fifth of the magnitude of the left matrix elements. The experimental log ft values in the left branch are

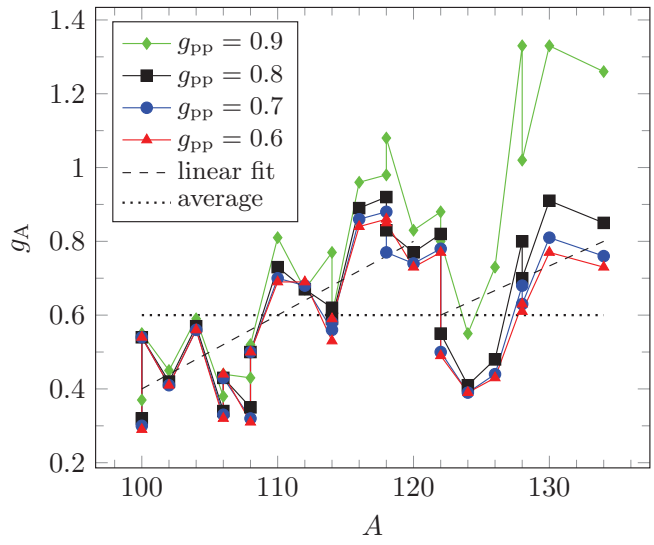

FIG. 3. (Color online) Values of g_A as a function of the mass number A. The data points were produced by fitting the theoretical geometric means of the NMEs to the corresponding experimental values.

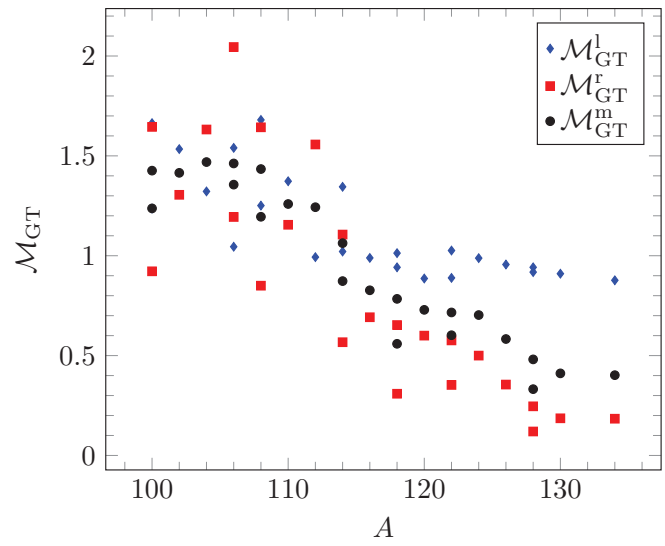

FIG. 4. (Color online) Theoretical β-decay matrix elements as a function of the mass number A. The computations were done with $g_{pp} = 0.7$. The effect of g_A has not yet been taken into account.

TABLE I. Experimental geometric means of the NMEs. The experimental values were taken from Ref. [52], except the entry marked with superscript [1] is extrapolated from systematics of similar neighboring decays and the entry marked with superscript [2] is from Ref. [53].

A	Z	Process			$\log ft_{\text{exp}}$		$g_{\text{A}}M_{\text{GT}}$(l)	$g_{\text{A}}M_{\text{GT}}$(r)	$g_{\text{A}}M^{\text{m}}_{\text{GT}}$
		Z	$Z+1$	$Z+2$	left	right			
100	40	$Zr(0^+)$	$\rightarrow Nb(1^+) \rightarrow$	$Mo(0^+)$	4.65	5.1	0.371	0.382	0.377
100	42	$Mo(0^+)$	$\leftarrow Tc(1^+) \rightarrow$	$Ru(0^+)$	4.4	4.59	0.857	0.688	0.768
102	42	$Mo(0^+)$	$\rightarrow Tc(1^+) \rightarrow$	$Ru(0^+)$	4.21	4.778	0.616	0.554	0.584
104	44	$Ru(0^+)$	$\leftarrow Rh(1^+) \rightarrow$	$Pd(0^+)$	4.32	4.55	0.939	0.721	0.823
106	44	$Ru(0^+)$	$\rightarrow Rh(1^+) \rightarrow$	$Pd(0^+)$	4.31	5.168	0.548	0.354	0.441
106	46	$Pd(0^+)$	$\leftarrow Ag(1^+) \rightarrow$	$Cd(0^+)$	4.92	4.4[1)]	0.471	0.857	0.635
108	44	$Ru(0^+)$	$\rightarrow Rh(1^+) \rightarrow$	$Pd(0^+)$	4.2[2)]	5.5	0.623	0.241	0.388
108	46	$Pd(0^+)$	$\leftarrow Ag(1^+) \rightarrow$	$Cd(0^+)$	4.70	4.425	0.607	0.833	0.711
110	46	$Pd(0^+)$	$\leftarrow Ag(1^+) \rightarrow$	$Cd(0^+)$	4.09	4.6596	1.224	0.635	0.882
112	48	$Cd(0^+)$	$\leftarrow In(1^+) \rightarrow$	$Sn(0^+)$	4.70	4.12	0.607	1.183	0.847
114	46	$Pd(0^+)$	$\rightarrow Ag(1^+) \rightarrow$	$Cd(0^+)$	4.199	5.1	0.623	0.383	0.488
114	48	$Cd(0^+)$	$\leftarrow In(1^+) \rightarrow$	$Sn(0^+)$	4.89	4.4701	0.487	0.790	0.621
116	48	$Cd(0^+)$	$\leftarrow In(1^+) \rightarrow$	$Sn(0^+)$	4.47	4.662	0.790	0.634	0.708
118	48	$Cd(0^+)$	$\rightarrow In(1^+) \rightarrow$	$Sn(0^+)$	3.91	4.79	0.870	0.547	0.690
118	50	$Sn(0^+)$	$\leftarrow Sb(1^+) \leftarrow$	$Te(0^+)$	4.525	5.0	0.742	0.248	0.429
120	48	$Cd(0^+)$	$\rightarrow In(1^+) \rightarrow$	$Sn(0^+)$	4.1	5.023	0.699	0.418	0.541
122	48	$Cd(0^+)$	$\rightarrow In(1^+) \rightarrow$	$Sn(0^+)$	3.95	5.11	0.830	0.378	0.561
122	52	$Te(0^+)$	$\leftarrow I(1^+) \leftarrow$	$Xe(0^+)$	4.95	5.191	0.455	0.199	0.301
124	54	$Xe(0^+)$	$\leftarrow Cs(1^+) \leftarrow$	$Ba(0^+)$	5.10	5.2	0.383	0.197	0.275
126	54	$Xe(0^+)$	$\leftarrow Cs(1^+) \leftarrow$	$Ba(0^+)$	5.066	5.36	0.398	0.164	0.255
128	52	$Te(0^+)$	$\leftarrow I(1^+) \rightarrow$	$Xe(0^+)$	5.049	6.061	0.406	0.127	0.227
128	54	$Xe(0^+)$	$\leftarrow Cs(1^+) \leftarrow$	$Ba(0^+)$	4.847	5.28	0.512	0.180	0.303
130	54	$Xe(0^+)$	$\leftarrow Cs(1^+) \rightarrow$	$Ba(0^+)$	5.073	5.36	0.395	0.284	0.335
134	56	$Ba(0^+)$	$\leftarrow La(1^+) \leftarrow$	$Ce(0^+)$	4.883	5.23	0.491	0.190	0.306

TABLE II. Theoretical and experimental geometric means of the NMEs with $g_{\text{pp}} = 0.7$. The values of g_{A} were fixed for each process by fitting the theoretical geometric mean to the experimental value.

A	Z	Process			g_{A}	$M^{\text{th}}_{\text{GT}}$(l)	$M^{\text{th}}_{\text{GT}}$(r)	$g_{\text{A}}M^{\text{m}}_{\text{GT}}$	
		Z	$Z+1$	$Z+2$				exp.	th.
100	40	$Zr(0^+)$	$\rightarrow Nb(1^+) \rightarrow$	$Mo(0^+)$	0.30	1.664	0.922	0.377	0.372
100	42	$Mo(0^+)$	$\leftarrow Tc(1^+) \rightarrow$	$Ru(0^+)$	0.54	1.236	1.645	0.768	0.770
102	42	$Mo(0^+)$	$\rightarrow Tc(1^+) \rightarrow$	$Ru(0^+)$	0.41	1.534	1.305	0.584	0.580
104	44	$Ru(0^+)$	$\leftarrow Rh(1^+) \rightarrow$	$Pd(0^+)$	0.56	1.322	1.632	0.823	0.823
106	44	$Ru(0^+)$	$\rightarrow Rh(1^+) \rightarrow$	$Pd(0^+)$	0.33	1.540	1.194	0.441	0.447
106	46	$Pd(0^+)$	$\leftarrow Ag(1^+) \rightarrow$	$Cd(0^+)$	0.43	1.045	2.045	0.635	0.629
108	44	$Ru(0^+)$	$\rightarrow Rh(1^+) \rightarrow$	$Pd(0^+)$	0.32	1.680	0.8502	0.388	0.382
108	46	$Pd(0^+)$	$\leftarrow Ag(1^+) \rightarrow$	$Cd(0^+)$	0.50	1.251	1.643	0.711	0.717
110	46	$Pd(0^+)$	$\leftarrow Ag(1^+) \rightarrow$	$Cd(0^+)$	0.70	1.373	1.155	0.882	0.882
112	48	$Cd(0^+)$	$\leftarrow In(1^+) \rightarrow$	$Sn(0^+)$	0.68	0.993	1.557	0.847	0.846
114	46	$Pd(0^+)$	$\rightarrow Ag(1^+) \rightarrow$	$Cd(0^+)$	0.56	1.345	0.5676	0.488	0.489
114	48	$Cd(0^+)$	$\leftarrow In(1^+) \rightarrow$	$Sn(0^+)$	0.58	1.021	1.106	0.621	0.616
116	48	$Cd(0^+)$	$\leftarrow In(1^+) \rightarrow$	$Sn(0^+)$	0.86	0.989	0.692	0.708	0.711
118	48	$Cd(0^+)$	$\rightarrow In(1^+) \rightarrow$	$Sn(0^+)$	0.88	0.942	0.653	0.690	0.690
118	50	$Sn(0^+)$	$\leftarrow Sb(1^+) \leftarrow$	$Te(0^+)$	0.77	1.013	0.309	0.429	0.430
120	48	$Cd(0^+)$	$\rightarrow In(1^+) \rightarrow$	$Sn(0^+)$	0.74	0.886	0.600	0.541	0.540
122	48	$Cd(0^+)$	$\rightarrow In(1^+) \rightarrow$	$Sn(0^+)$	0.78	0.889	0.576	0.561	0.558
122	52	$Te(0^+)$	$\leftarrow I(1^+) \leftarrow$	$Xe(0^+)$	0.50	1.026	0.353	0.301	0.301
124	54	$Xe(0^+)$	$\leftarrow Cs(1^+) \leftarrow$	$Ba(0^+)$	0.39	0.988	0.500	0.275	0.274
126	54	$Xe(0^+)$	$\leftarrow Cs(1^+) \leftarrow$	$Ba(0^+)$	0.44	0.956	0.355	0.255	0.256
128	52	$Te(0^+)$	$\leftarrow I(1^+) \rightarrow$	$Xe(0^+)$	0.68	0.918	0.120	0.227	0.226
128	54	$Xe(0^+)$	$\leftarrow Cs(1^+) \leftarrow$	$Ba(0^+)$	0.63	0.942	0.246	0.303	0.304
130	54	$Xe(0^+)$	$\leftarrow Cs(1^+) \rightarrow$	$Ba(0^+)$	0.81	0.910	0.186	0.335	0.333
134	56	$Ba(0^+)$	$\leftarrow La(1^+) \leftarrow$	$Ce(0^+)$	0.76	0.877	0.184	0.306	0.305

generally smaller than the log ft values in the right branch, so this is in good agreement with the experimentally observed behavior.

In Fig. 3 one can immediately see that, with respect to increase in g_{pp}, g_A becomes more unstable with increasing A. The value of $g_{pp} = 0.9$ is thus discarded as only a small variation in g_A is desired. It is also evident, given a reasonable interval of g_{pp} values, that the geometric mean does not depend very much on the value of g_{pp} as was expected. This can be seen in Fig. 3 as the data points representing different values of g_{pp} for a given nucleus are very close to each other. In other words, it does not take a significant change in g_A to compensate for a relatively large change in g_{pp}.

Interestingly enough, the calculations replicate the experimental geometric means of the NMEs for $g_{pp} = 0.6, 0.7, 0.8$ only for values of $g_A < 1$. This is solid evidence that an effective g_A is needed when working with this mass region. Not only are the values in general smaller than the bare value of $g_A = 1.25$ but in some cases an effective value as low as $g_A = 0.3$ is required.

In Fig. 3 one can see an interesting rising behavior in g_A as a function of A. There seem to be two mass regions in which g_A behaves, on average, linearly with a positive slope. The average linear behavior is depicted in the figure as two dashed lines. These lines are represented by

$$g_A = \begin{cases} 0.02A - 1.6, & \text{for} \quad A \in [100, 120] \\ \frac{1}{60}A - \frac{43}{30}, & \text{for} \quad A \in [122, 134] \end{cases} . \tag{28}$$

By using this function to generate values of g_A and adopting a reasonably average value of $g_{pp} = 0.7$ across the entire mass region, the Gamow-Teller matrix elements were calculated for the ground-state-to-ground-state decays. The resulting left and right log ft values are presented in Figs. 5 and 6 respectively along with results of the same calculation made with an average constant value of $g_A = 0.6$ for comparison. The linear model appears to fare better overall in predicting the log ft values of single-β decays, especially in the right branch decays. The agreement with experiment is decent at the very least. The decays which are not quite along the line of Eq. (28) in Fig. 3 expectedly produce somewhat less accurate predictions, for example, the $A = 124$ triplet.

To evaluate the success of the linear model, the mean deviation of the theoretical log ft values from the experimental ones was used as a quality value. The mean deviation reads:

$$\Delta_m = \frac{1}{\#D} \sum_D |\log ft_{th} - \log ft_{exp}| , \tag{29}$$

where the summation is over all of the investigated decay processes. The mean deviations for the linear g_A model yield $\Delta_m = 0.27, 0.18, 0.23$ for the left branch, right branch, and all decays, respectively. For the constant $g_A = 0.6$ the corresponding numbers are $\Delta_m = 0.27, 0.30, 0.29$. The linear model fares even better in the $A = 100$–120 region, where the mean deviations are $\Delta_m = 0.22, 0.14, 0.18$, while we get $\Delta_m = 0.28, 0.28, 0.28$ for the constant g_A. The use of this linear g_A is thus feasible as the overall accuracy of the predictions is very good for such a simple model.

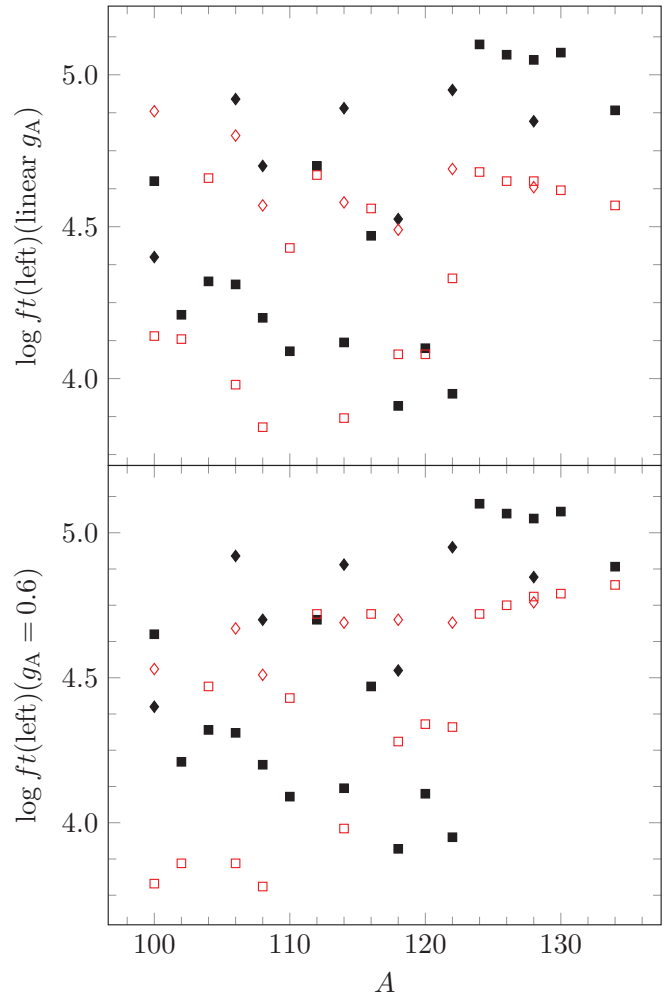

FIG. 5. (Color online) Experimental and theoretical log ft values of the ground-state-to-ground-state left branch single-β decays across the examined mass region. The computations were made with $g_{pp} = 0.7$ using the linear g_A model (upper panel) and a constant value of $g_A = 0.6$ (lower panel). Solid black and hollow red (gray) symbols are used to represent the experimental and theoretical log ft values, respectively. Different symbols are used to distinguish different decay processes within the same mass number.

The examination of the linear g_A model was then extended to decays from the 1^+ ground state of the odd-odd nuclei to the first excited 2^+ state of the even-even nuclei and to the 0^+ and 2^+ two-phonon states constructed from the wave function of the first 2^+ state.

All processes in the investigated mass region with experimental data available for decays to these excited states have been included and the resulting log ft values are visualized in Figs. 7–9. The results with $g_A = 0.6$ have again been included in the figures for reference. The predictions of log ft values for decays beyond ground states are generally more tricky. The QRPA and pnQRPA calculations are often accurate for only the lowest-lying states and even then the wave function of the obtained state might connect to some other state with the same angular momentum and parity, perhaps at a higher energy. The

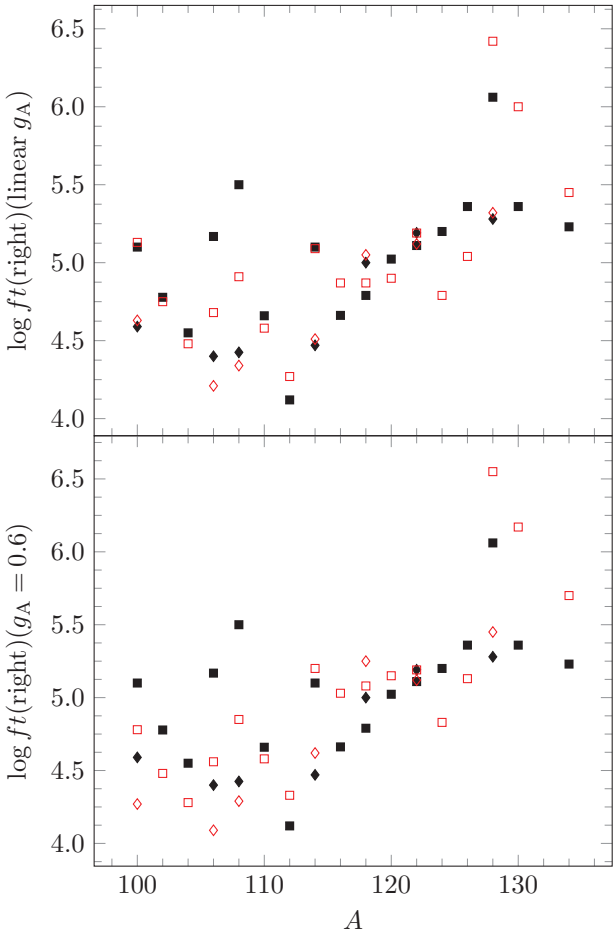

FIG. 6. (Color online) Same as Fig. 5 for the right branch decays.

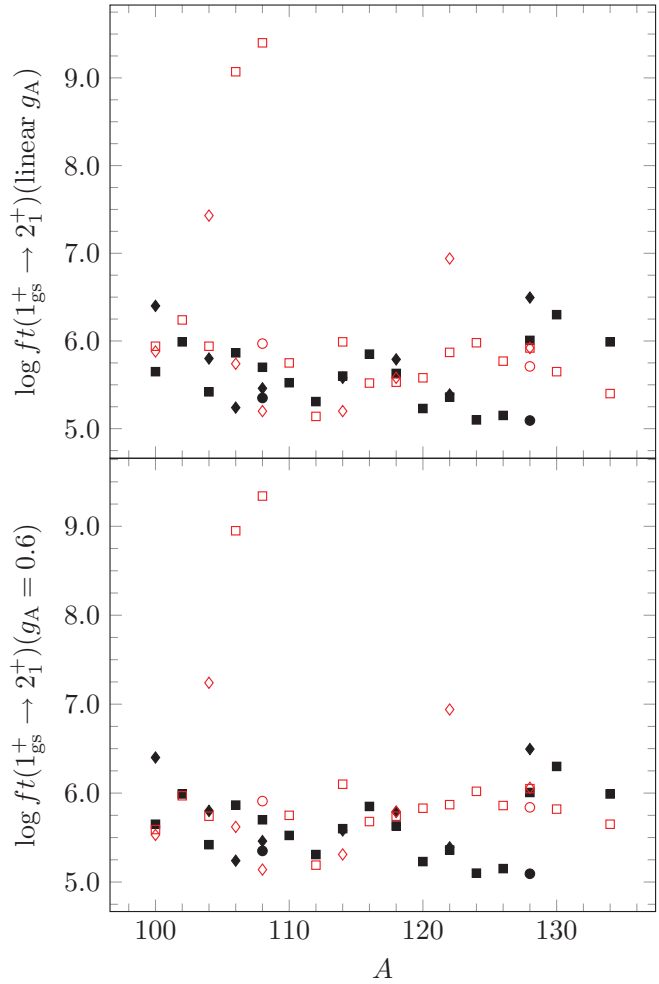

FIG. 7. (Color online) Experimental and theoretical log ft values of decays to the first excited 2^+ states of the even-even nuclei. The computations were made with $g_{pp} = 0.7$ using the linear g_A model (upper panel) and a constant value of $g_A = 0.6$ (lower panel). Solid black and hollow red (gray) symbols are used to represent the experimental and theoretical log ft values, respectively. Different symbols are used to distinguish different decay processes within the same mass number.

assumption of the simple structure (25) of the two-phonon states is one more limitation of the present model.

Still, the accuracy of the prediction is quite passable, especially for decays to the first 2^+ state, the energy of which was fitted to the experimental value. The calculated log ft values for decays to the two-phonon 2^+ state are systematically too large compared to the experimental values. For these states the assumed simple two-phonon structure seems to be inadequate.

A curious case arises in the decay of rhodium to palladium via β^- decay, in which the transition to the first 2^+ state is predicted very slow for each $A = 104, 106, 108$. This can be seen in Fig. 7 as the largest deviations from the experimental values. The deviation arises from subtle cancellations among the pnQRPA X and Y amplitudes in the major components of the wave function of the ground state of the Rh nucleus and the QRPA amplitudes of the first 2^+ state of the even-even reference nucleus. There are thus large cancellations in the transition amplitudes and the calculated log ft values are very high, making the comparative half-lives too long by several orders of magnitude.

The mean deviations in decays to excited states using the linear g_A model are $\Delta_m = 0.75, 0.70, 0.81$ for decays to the 2^+_1, 0^+_{2-ph}, and 2^+_{2-ph} states respectively. For the constant value, $g_A = 0.6$, the corresponding numbers are $\Delta_m = 0.70, 0.79, 0.88$. A major part of the deviation of the 2^+_1 case comes from the three rhodium to palladium decays which do not function well in the theoretical framework. With those three processes excluded, we find the mean deviations to be $\Delta_m = 0.47, 0.70, 0.83$ for the linear model, and $\Delta_m = 0.43, 0.79, 0.91$ for the constant g_A.

The constant g_A seems actually preferable for the decay to the first 2^+ state, but for the two-phonon states the linear model is again more accurate. This is quite peculiar, as the two-phonon states are formed from the one-phonon 2^+ state. It appears that the decays to excited states follow some other g_A systematic than the ground-state-to-ground-state decays. The standard QRPA framework is clearly not an accurate framework for depicting these transitions.

A disappearance of a clear two-phonon 0^+ state happens at $A \geqslant 126$. The experimental log ft values used in Fig. 8 are for the lowest excited 0^+ state, but this state is always too

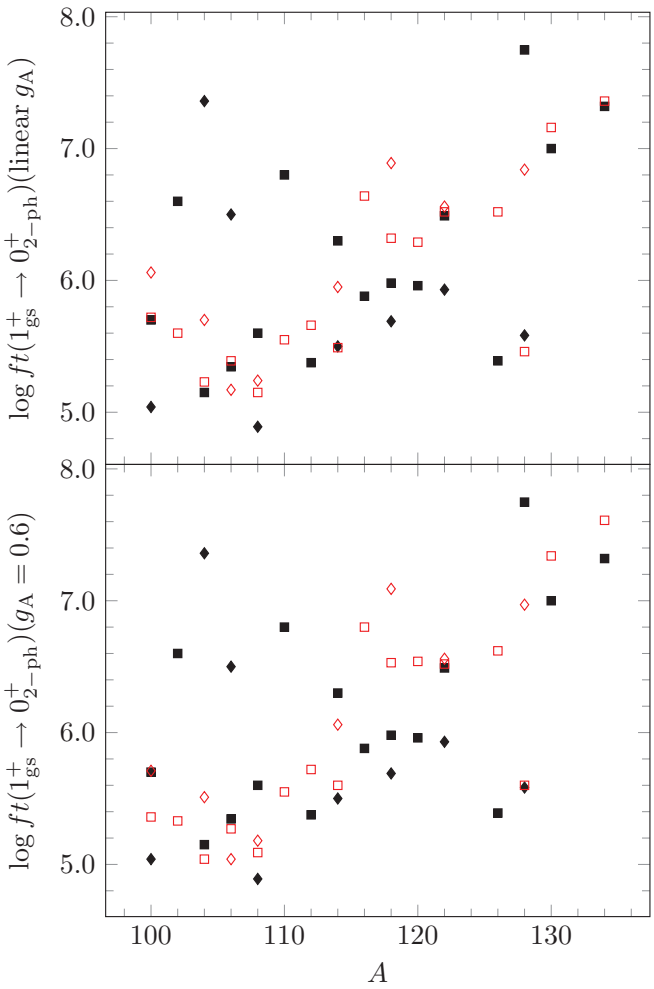

FIG. 8. (Color online) Same as Fig. 7 for decays to the 0^+ quadrupole two-phonon states of the even-even nuclei.

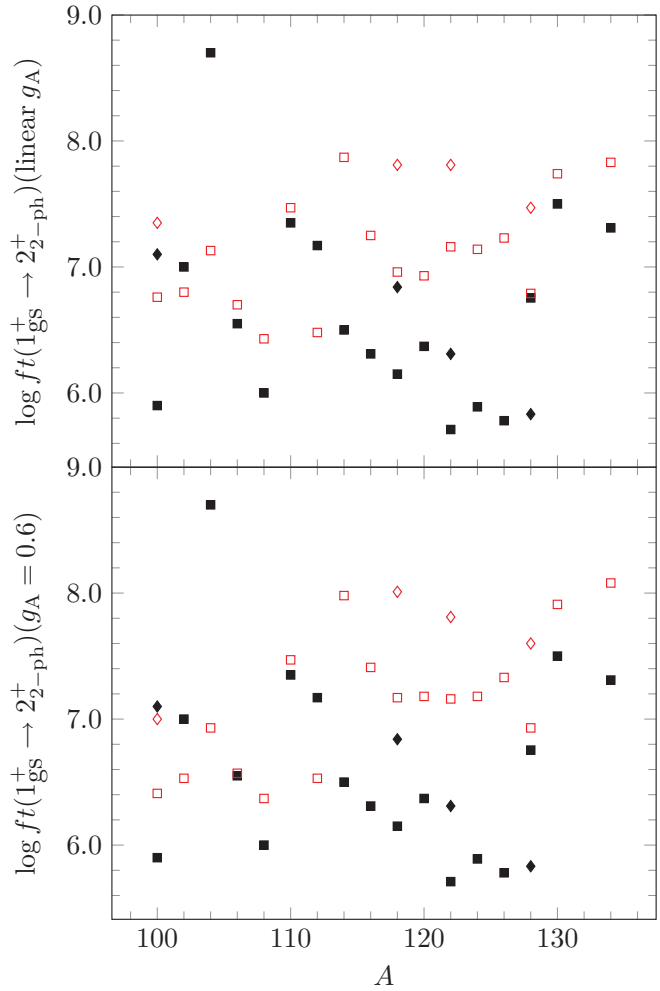

FIG. 9. (Color online) Same as Fig. 7 for decays to the 2^+ quadrupole two-phonon states of the even-even nuclei.

high in energy to be the two-phonon state the theory predicts. Either the breaking of the degeneracy of the collective two-phonon triplet increases with increasing mass number A or the formation of this particular multipolarity is prevented by some mechanism in nuclei investigated here with $A \geqslant 126$. The theoretical log ft values for these transitions often seem to deviate more than one unit from the experimental log ft value for the 0^+_2 state. This makes it more probable for the lowest excited experimental 0^+ state to result from some other origin than two quadrupole phonons.

The β-decay rates in the $A = 104$ and $A = 110$ systems were also calculated in Ref. [30]. The computed log ft values of the present work are compared to these results in Table III. In Ref. [30] the transition rates were also computed using adjusted single-particle bases where the Woods-Saxon energies of some orbitals had been altered to better replicate experimental values. The comparison is made between results computed using the plain Woods-Saxon bases as was used in the present work. The results appear quite similar. Our present analysis predicts the ground-state-to-ground-state decays slightly more accurately. The computations of Ref. [30] systematically yield too fast transition rates while the present work gives more balanced results. The use of adjusted single-particle orbitals might enhance the accuracy of our present predictions as it did in Ref. [30].

TABLE III. Single-β decay log ft values compared with those of Ref. [30].

Transition		J^π_f	log ft			
			Exp.	Ref. [30]	Linear g_A	$g_A = 0.60$
^{104}Rh $\to$	^{104}Pd	0^+_{gs}	4.55	4.32	4.48	4.28
		2^+_1	5.80	6.50	7.43	7.24
		0^+_2	7.36	5.08	5.70	5.51
		2^+_2	8.7	6.85	7.13	6.93
^{104}Rh $\to$	^{104}Ru	0^+_{gs}	4.32	3.73	4.66	4.47
		2^+_1	5.42	5.35	5.94	5.74
		0^+_2	5.15	4.63	5.23	5.04
^{110}Ag $\to$	^{110}Cd	0^+_{gs}	4.66	4.84	4.58	4.58
		2^+_1	5.52	5.46	5.75	5.75
		0^+_2	6.80	5.02	5.55	5.55
		2^+_2	7.35	7.52	7.47	7.47
^{110}Ag $\to$	^{110}Pd	0^+_{gs}	4.09	3.72	4.43	4.43

TABLE IV. The phase-space integrals used in calculating the $2\nu\beta\beta$ matrix elements for different final states. The effect of g_A is included in the tabulated values. In the cases of double-positron decay, only modes with nonzero phase-space factors have been included.

Transition	g_A	Mode	Phase-space integral (J_f^π)			
			0^+_{gs}	2^+_1	0^+_2	2^+_2
^{100}Mo → ^{100}Ru	0.40	$\beta^-\beta^-$	9.907×10^{-20}	1.892×10^{-20}	1.836×10^{-21}	1.331×10^{-22}
^{104}Ru → ^{104}Pd	0.48	$\beta^-\beta^-$	2.017×10^{-22}	2.044×10^{-26}		
^{110}Pd → ^{110}Cd	0.60	$\beta^-\beta^-$	2.125×10^{-20}	7.608×10^{-23}	6.985×10^{-25}	1.400×10^{-27}
^{114}Cd → ^{114}Sn	0.68	$\beta^-\beta^-$	1.302×10^{-24}			
^{116}Cd → ^{116}Sn	0.72	$\beta^-\beta^-$	8.788×10^{-19}	7.014×10^{-22}	2.687×10^{-22}	6.477×10^{-26}
^{122}Sn → ^{122}Te	0.60	$\beta^-\beta^-$	5.767×10^{-26}			
^{124}Sn → ^{124}Te	0.63	$\beta^-\beta^-$	1.095×10^{-19}	1.890×10^{-21}	4.080×10^{-24}	2.316×10^{-24}
^{128}Te → ^{128}Xe	0.70	$\beta^-\beta^-$	8.668×10^{-23}			
^{130}Te → ^{130}Xe	0.73	$\beta^-\beta^-$	5.623×10^{-19}	3.323×10^{-20}	3.010×10^{-23}	4.828×10^{-22}
^{134}Xe → ^{134}Ba	0.80	$\beta^-\beta^-$	1.491×10^{-22}	1.176×10^{-30}		
^{136}Xe → ^{136}Ba	0.83	$\beta^-\beta^-$	9.444×10^{-19}	7.024×10^{-21}	2.748×10^{-22}	6.834×10^{-24}
^{102}Pd → ^{102}Ru	0.44	β^+EC(K)	6.277×10^{-33}			
		β^+EC(L)	3.816×10^{-33}			
		ECEC(KK)	3.704×10^{-25}		2.990×10^{-29}	
		ECEC(KL)	1.161×10^{-25}	1.500×10^{-29}	1.601×10^{-29}	1.159×10^{-38}
^{106}Cd → ^{106}Pd	0.52	$\beta^+\beta^+$	1.408×10^{-27}	8.369×10^{-38}		
		β^+EC(K)	1.190×10^{-23}	9.297×10^{-24}	3.925×10^{-27}	8.249×10^{-27}
		β^+EC(L)	1.838×10^{-24}	1.633×10^{-24}	7.406×10^{-28}	8.249×10^{-27}
		ECEC(KK)	8.768×10^{-23}		5.869×10^{-24}	
		ECEC(KL)	2.555×10^{-23}	2.171×10^{-25}	1.764×10^{-24}	2.247×10^{-26}
^{108}Cd → ^{108}Pd	0.56	ECEC(KK)	2.910×10^{-28}			
		ECEC(KL)	1.411×10^{-28}			
^{112}Sn → ^{112}Cd	0.64	β^+EC(K)	1.813×10^{-25}	2.673×10^{-30}		
		β^+EC(L)	3.191×10^{-26}	1.116×10^{-30}		
		ECEC(KK)	4.209×10^{-23}		1.882×10^{-25}	
		ECEC(KL)	1.271×10^{-23}	1.550×10^{-26}	6.492×10^{-26}	5.590×10^{-29}
^{120}Te → ^{120}Sn	0.80	β^+EC(K)	5.109×10^{-26}			
		β^+EC(L)	1.009×10^{-26}			
		ECEC(KK)	7.506×10^{-23}			
		ECEC(KL)	2.326×10^{-23}	7.167×10^{-29}		
^{124}Xe → ^{124}Te	0.63	$\beta^+\beta^+$	7.279×10^{-27}	6.817×10^{-38}		
		β^+EC(K)	5.590×10^{-23}	2.741×10^{-23}	1.448×10^{-31}	2.689×10^{-27}
		β^+EC(L)	9.119×10^{-24}	5.326×10^{-24}	1.086×10^{-31}	7.704×10^{-28}
		ECEC(KK)	6.072×10^{-22}		6.592×10^{-24}	
		ECEC(KL)	1.844×10^{-22}	2.179×10^{-24}	2.170×10^{-24}	1.367×10^{-25}
^{126}Xe → ^{126}Te	0.67	ECEC(KK)	1.217×10^{-24}			
		ECEC(KL)	5.328×10^{-25}	7.746×10^{-32}		
^{130}Ba → ^{130}Xe	0.73	$\beta^+\beta^+$	1.321×10^{-28}			
		β^+EC(K)	3.179×10^{-23}	7.334×10^{-24}		7.339×10^{-28}
		β^+EC(L)	5.453×10^{-24}	1.583×10^{-24}		2.649×10^{-28}
		ECEC(KK)	8.788×10^{-22}		1.521×10^{-24}	
		ECEC(KL)	2.733×10^{-22}	3.180×10^{-24}	5.604×10^{-25}	2.767×10^{-25}
^{132}Ba → ^{132}Xe	0.77	ECEC(KK)	2.546×10^{-24}			
		ECEC(KL)	9.256×10^{-25}	5.568×10^{-33}		
^{136}Ce → ^{136}Ba	0.83	$\beta^+\beta^+$	1.718×10^{-30}			
		β^+EC(K)	2.273×10^{-23}	1.887×10^{-26}		
		β^+EC(L)	4.079×10^{-24}	5.913×10^{-27}		
		ECEC(KK)	1.375×10^{-21}		4.177×10^{-24}	
		ECEC(KL)	4.363×10^{-22}	1.265×10^{-24}	1.564×10^{-24}	1.266×10^{-26}

C. Half-lives of double β decays

The half-life of every possible two-neutrino double-β decay in the examined mass region was calculated using the g_A scheme of Eq. (28). The calculation was also done with a constant value of $g_A = 0.6$ for comparison. For the particle-particle interaction parameter we adopted the value of $g_{pp} = 0.7$, which functioned quite well in predicting the single-β decay comparative half-lives. One should note here

TABLE V. Theoretical NMEs (columns 2–5) and half-lives (columns 7–10) of double-β^--type decays with the linear g_A model and $g_A = 0.6$ (column 6), using $g_{pp} = 0.7$. Contributions from the first intermediate state only are in parentheses below the NMEs calculated using all contributions. The computation for ^{136}Xe was made for (a) $E_{1_1^+} = 0.0$ MeV and (b) $E_{1_1^+} = 1.0$ MeV. The experimental half-lives (column 11) are from Ref. [54] and the lower limits from Ref. [55].

Nucleus	$\lvert M_{2\nu}\rvert$				g_A	$t_{1/2}^{(2\nu)}$(y)				$t_{1/2}^{\text{exp.}}$(y)
	0^+_{gs}	2^+_1	0^+_{2-ph}	2^+_{2-ph}		0^+_{gs}	2^+_1	0^+_{2-ph}	2^+_{2-ph}	
^{100}Mo	0.6560	0.0227	0.1150	0.0028	0.40	2.3×10^{19}	1.0×10^{23}	4.1×10^{22}	9.8×10^{26}	$(7.1 \pm 0.4) \times 10^{18}$
	(0.618)	(0.0227)	(0.0993)	(0.0028)	0.60	4.6×10^{18}	2.0×10^{22}	8.1×10^{21}	1.9×10^{26}	
^{104}Ru	0.6520	0.0026	0.1381	0.0026	0.48	1.2×10^{22}	7.1×10^{30}			
	(0.615)	(0.0025)	(0.124)	(0.0026)	0.60	4.8×10^{21}	2.9×10^{30}			
^{110}Pd	0.4651	0.0149	0.1415	0.0015	0.60	2.2×10^{20}	5.9×10^{25}	7.1×10^{25}	3.1×10^{32}	$>6.0 \times 10^{16}$
	(0.429)	(0.0150)	(0.122)	(0.0016)	0.60	2.2×10^{20}	5.9×10^{25}	7.1×10^{25}	3.1×10^{32}	
^{114}Cd	0.3829	0.0568	0.0961	0.0445	0.68	5.2×10^{24}				$>9.2 \times 10^{16}$
	(0.342)	(0.0576)	(0.0912)	(0.0445)	0.60	8.6×10^{24}				
^{116}Cd	0.2169	0.0238	0.0483	0.0103	0.72	2.4×10^{19}	2.5×10^{24}	1.6×10^{24}	1.4×10^{29}	$(2.85 \pm 0.15) \times 10^{19}$
	(0.188)	(0.0236)	(0.0453)	(0.0103)	0.60	5.0×10^{19}	5.2×10^{24}	3.3×10^{24}	3.0×10^{29}	
^{122}Sn	0.07515	0.0102	0.2016	0.0014	0.60	3.1×10^{27}				
	(0.0298)	(0.0106)	(0.0881)	(0.0019)	0.60	3.1×10^{27}				
^{124}Sn	0.0575	0.0100	0.1727	0.0018	0.63	2.8×10^{21}	5.3×10^{24}	8.2×10^{24}	1.4×10^{29}	$>1.0 \times 10^{17}$
	(0.0204)	(0.0103)	(0.0737)	(0.0023)	0.60	3.4×10^{21}	6.4×10^{24}	1.0×10^{25}	1.7×10^{29}	
^{128}Te	0.1041	0.0082	0.1951	0.0012	0.70	1.1×10^{24}				$(2.0 \pm 0.3) \times 10^{24}$
	(0.0303)	(0.0085)	(0.0730)	(0.0020)	0.60	2.0×10^{24}				
^{130}Te	0.1066	0.0085	0.2145	0.0014	0.73	1.6×10^{20}	4.2×10^{23}	7.2×10^{23}	1.0×10^{27}	$(6.9 \pm 1.3) \times 10^{20}$
	(0.0320)	(0.0084)	(0.0862)	(0.0024)	0.60	3.4×10^{20}	9.1×10^{23}	1.6×10^{24}	2.2×10^{27}	
^{134}Xe	0.0979	0.0029	0.1738	0.0007	0.80	7.0×10^{23}	9.9×10^{34}			$>1.1 \times 10^{16}$
	(0.0270)	(0.0023)	(0.0589)	(0.0016)	0.60	2.2×10^{24}	3.1×10^{35}			
^{136}Xe (a)	0.0532	0.0003	0.1675	0.0003	0.83	3.7×10^{20}	1.6×10^{25}	1.3×10^{23}	1.2×10^{30}	$(2.20 \pm 0.06) \times 10^{21}$
	(0.0016)	(0.0003)	(0.00003)	(0.00001)	0.60	1.4×10^{21}	5.9×10^{25}	4.7×10^{23}	4.3×10^{30}	
^{136}Xe (b)	0.0405	0.0010	0.1224	0.0003	0.83	6.5×10^{20}	1.3×10^{26}	2.4×10^{23}	1.7×10^{30}	$(2.20 \pm 0.06) \times 10^{21}$
	(0.0009)	(0.00004)	(9×10^{-6})	(4×10^{-7})	0.60	2.4×10^{21}	4.8×10^{26}	8.9×10^{23}	6.3×10^{30}	

that although this value of g_{pp} works well for the geometric means of the left- and right-side NMEs, it does not remove the ambiguity of g_{pp} for individual NMEs. Eleven β^--type and 10 β^+/EC-type processes were examined. The phase-space integrals used to calculate the double-β decay matrix elements are tabulated in Table IV. The calculated matrix elements and half-lives for the β^- processes are presented in Table V and for the β^+/EC mode decays are in Table VII for systems with $A \leqslant 120$ and Table VIII for $A \geqslant 124$. It should be noted that half-lives are given only for processes that are allowed by positive Q value while the values of the NMEs are calculated nevertheless.

The success of our predictions can only be evaluated by the experimental half-lives known for five $\beta^-\beta^-$ processes. The

TABLE VI. Theoretical and experimental half-lives of double β^- type decays computed with the linear g_A model along with constant $g_A = 0.6$. The computation for ^{136}Xe was made for (a) $E_{1_1^+} = 0.0$ MeV and (b) $E_{1_1^+} = 1.0$ MeV. The experimental half-lives are from Ref. [54]. A quality value (see text) of each result is presented in the last column.

Nucleus	g_A	$t_{1/2}^{\text{th}}(0^+_{gs})$(y)	$t_{1/2}^{\text{exp}}(0^+_{gs})$(y)	Quality
^{100}Mo	0.40	2.3×10^{19}	$(7.1 \pm 0.4) \times 10^{18}$	2.2
	0.60	4.6×10^{18}		0.4
^{116}Cd	0.72	2.4×10^{19}	$(2.85 \pm 0.15) \times 10^{19}$	0.2
	0.60	5.0×10^{19}		0.8
^{128}Te	0.70	1.1×10^{24}	$(2.0 \pm 0.3) \times 10^{24}$	0.5
	0.60	2.0×10^{24}		0.0
^{130}Te	0.73	1.6×10^{20}	$(6.9 \pm 1.3) \times 10^{20}$	0.8
	0.60	3.4×10^{20}		0.5
^{136}Xe (a)	0.83	3.7×10^{20}	$(2.20 \pm 0.06) \times 10^{21}$	0.8
	0.60	1.4×10^{21}		0.4
^{136}Xe (b)	0.83	6.5×10^{20}	$(2.20 \pm 0.06) \times 10^{21}$	0.7
	0.60	2.4×10^{21}		0.1

TABLE VII. Theoretical NMEs (columns 3–6) and half-lives (columns 8–11) for double positron decays for $A \leqslant 120$. The computations were made with the linear g_A model and $g_A = 0.6$ (column 7), using $g_{pp} = 0.7$. Contributions from the first intermediate state only are in parentheses below the NMEs calculated using all contributions. The matrix elements given for processes including electron capture are mean values of the K capture and L capture or KK and KL matrix elements.

Nucleus	Type	$\lvert M_{2\nu}\rvert$				g_A	$t_{1/2}$(y)			
		0^+_{gs}	2^+_1	0^+_{2-ph}	2^+_{2-ph}		0^+_{gs}	2^+_1	0^+_{2-ph}	2^+_{2-ph}
^{102}Pd	$\beta^+\beta^+$	0.7348	0.0008	0.28551	0.0097	0.44				
		(0.7287)	(0.0006)	(0.2833)	(0.0097)	0.60				
	β^+EC	1.5256	0.0009	0.5830	0.0144	0.44	4.3×10^{31}			
		(1.5135)	(0.0007)	(0.5786)	(0.0143)	0.60	1.2×10^{31}			
	ECEC	1.4697	0.0009	0.5710	0.0139	0.44	9.5×10^{23}	8.8×10^{34}	6.7×10^{28}	4.5×10^{41}
		(1.4574)	(0.0007)	(0.5666)	(0.0138)	0.60	2.8×10^{23}	2.5×10^{34}	1.9×10^{28}	1.3×10^{41}
^{106}Cd	$\beta^+\beta^+$	0.9355	0.0186	0.4061	0.0209	0.52	8.1×10^{26}	3.5×10^{40}		
		(0.9342)	(0.0184)	(0.4042)	(0.0208)	0.60	4.6×10^{26}	1.9×10^{40}		
	β^+EC	2.2052	0.0313	0.9865	0.0477	0.52	1.5×10^{22}	9.5×10^{25}	2.2×10^{26}	4.5×10^{28}
		(2.2031)	(0.0311)	(0.9825)	(0.0476)	0.60	8.5×10^{21}	5.3×10^{25}	1.3×10^{26}	2.5×10^{28}
	ECEC	1.8710	0.0221	0.8123	0.0323	0.52	2.5×10^{21}	9.4×10^{27}	2.0×10^{23}	4.3×10^{28}
		(1.8685)	(0.0219)	(0.8084)	(0.0323)	0.60	1.4×10^{21}	5.3×10^{27}	1.1×10^{23}	2.4×10^{28}
^{108}Cd	$\beta^+\beta^+$	0.8132	0.0175	0.2270	0.0072	0.56				
		(0.8048)	(0.0175)	(0.2260)	(0.0072)	0.60				
	β^+EC	1.6474	0.0202	0.4541	0.0098	0.56				
		(1.6306)	(0.0202)	(0.4523)	(0.0098)	0.60				
	ECEC	1.6265	0.0200	0.4540	0.0098	0.56	8.7×10^{26}			
		(1.6097)	(0.0199)	(0.4521)	(0.0098)	0.60	6.6×10^{26}			
^{112}Sn	$\beta^+\beta^+$	0.7843	0.0288	0.1488	0.0096	0.64				
		(0.7841)	(0.0288)	(0.1481)	(0.0096)	0.60				
	β^+EC	1.7170	0.0422	0.3208	0.0186	0.64	1.6×10^{24}	1.5×10^{32}		
		(1.7167)	(0.0422)	(0.3196)	(0.0186)	0.60	2.1×10^{24}	1.9×10^{32}		
	ECEC	1.5686	0.0356	0.2975	0.0161	0.64	7.4×10^{21}	5.1×10^{28}	4.5×10^{25}	6.9×10^{31}
		(1.5683)	(0.0356)	(0.2963)	(0.0161)	0.60	9.6×10^{21}	6.6×10^{28}	5.8×10^{25}	9.0×10^{31}
^{120}Te	$\beta^+\beta^+$	0.1061	0.0013	0.0031	0.0003	0.80				
		(0.0666)	(0.0017)	(0.0030)	(0.0003)	0.60				
	β^+EC	0.2210	0.0022	0.0063	0.0007	0.80	3.4×10^{26}			
		(0.1414)	(0.0026)	(0.0062)	(0.0007)	0.60	1.1×10^{27}			
	ECEC	0.2122	0.0020	0.0062	0.0007	0.80	2.3×10^{23}	3.5×10^{33}		
		(0.1333)	(0.0024)	(0.0061)	(0.0007)	0.60	7.1×10^{23}	1.1×10^{34}		

computed and experimental half-lives of the ground-state-to-ground-state decays of these nuclei are tabulated separately in Table VI. In only one of these cases the experimental half-life is better reproduced by our linear g_A model than the constant value as seen in Table VI, namely, the decay of ^{116}Cd. The largest deviations from the experimental half-lives with the linear model appear in the decays of ^{100}Mo and ^{136}Xe where the discrepancy is of a factor of 3–6. One must bear in mind, though, that the $A = 136$ process is an extrapolation of our linear g_A model and the results must be considered with caution.

To compare the linear model and constant g_A we introduce a quality factor, which reads

$$\Delta = \frac{\left|t^{th}_{1/2} - t^{exp}_{1/2}\right|}{t^{exp}_{1/2}} . \tag{30}$$

These calculated quality factors are presented in Table VI for each decay process with experimental data available. The mean of the individual quality factors yields $\langle\Delta\rangle = 0.86$ for the linear g_A model and $\langle\Delta\rangle = 0.34$ for the constant $g_A = 0.6$. It seems that the $2\nu\beta^-\beta^-$ decay favors the constant $g_A = 0.6$ instead of one fitted via the systematics of single-β decay. Even with a function which more closely follows the zigzag behavior of Fig. 3 one would not find much improvement, as some of the predictions would essentially be corrected in the wrong direction. For example, the half-life of the ^{130}Te decay is already predicted as too short by the linear model and taking the exact value from Fig. 3 would lead to a larger g_A which in turn would lead to an even shorter half-life. In the basic QRPA framework, the single- and double-β decays seem to follow somewhat different g_A schemes as pointed out in Refs. [37,38] already.

For the processes with experimental data available, we find that the calculated half-lives are not very far off the experimental values for either the linear or the constant g_A. One might thus assume that a within-order-of-magnitude level of accuracy holds also for the processes with yet unmeasured half-lives. Of the processes with no present experimental data available, the ground-state-to-ground-state decay of ^{110}Pd, with a predicted half-life of 2.2×10^{20} years appears the most attractive for future experimental probing.

TABLE VIII. Theoretical NMEs (columns 3–6) and half-lives (columns 8–11) for double positron decays for $A \geqslant 124$. The computations were made with the linear g_A model and $g_A = 0.6$ (column 7), using $g_{pp} = 0.7$. Contributions from the first intermediate state only are in parentheses below the NMEs calculated using all contributions. The matrix elements given for processes including electron capture are mean values of the K capture and L capture or KK and KL matrix elements.

Nucleus	Type	$\lvert M_{2\nu}\rvert$				g_A	$t_{1/2}$(y)			
		0^+_{gs}	2^+_1	0^+_{2-ph}	2^+_{2-ph}		0^+_{gs}	2^+_1	0^+_{2-ph}	2^+_{2-ph}
^{124}Xe	$\beta^+\beta^+$	0.1480	0.0006	0.0045	5×10^{-5}	0.63	6.3×10^{27}	3.6×10^{43}		
		(0.0658)	(0.0006)	(0.0043)	(6×10^{-5})	0.60	7.6×10^{27}	4.3×10^{43}		
	β^+EC	0.3066	0.0008	0.0095	8×10^{-5}	0.63	1.6×10^{23}	4.6×10^{28}	4.4×10^{34}	4.6×10^{34}
		(0.1403)	(0.0008)	(0.0091)	(9×10^{-5})	0.60	2.0×10^{23}	5.5×10^{28}	5.4×10^{34}	5.6×10^{34}
	ECEC	0.2960	0.0007	0.0091	7×10^{-5}	0.63	1.4×10^{22}	8.6×10^{29}	1.4×10^{27}	1.4×10^{33}
		(0.1315)	(0.0007)	(0.0087)	(8×10^{-5})	0.60	1.8×10^{22}	1.0×10^{30}	1.7×10^{27}	1.7×10^{33}
^{126}Xe	$\beta^+\beta^+$	0.1365	0.0008	0.0028	5×10^{-5}	0.67				
		(0.0538)	(0.0006)	(0.0024)	(6×10^{-5})	0.60				
	β^+EC	0.2762	0.0009	0.0056	8×10^{-5}	0.67				
		(0.1102)	(0.0007)	(0.0048)	(10×10^{-5})	0.60				
	ECEC	0.2731	0.0009	0.0056	8×10^{-5}	0.67	7.7×10^{24}	1.6×10^{37}		
		(0.1077)	(0.0007)	(0.0048)	(9×10^{-5})	0.60	1.2×10^{25}	2.4×10^{37}		
^{130}Ba	$\beta^+\beta^+$	0.1757	0.0017	0.0039	10×10^{-5}	0.73	2.5×10^{29}			
		(0.0691)	(0.0014)	(0.0035)	(11×10^{-5})	0.60	5.4×10^{29}			
	β^+EC	0.3721	0.0024	0.0086	19×10^{-5}	0.73	1.9×10^{23}	2.0×10^{28}		2.9×10^{34}
		(0.1557)	(0.0021)	(0.0078)	(21×10^{-5})	0.60	4.3×10^{23}	4.3×10^{28}		6.3×10^{34}
	ECEC	0.3514	0.0019	0.0077	14×10^{-5}	0.73	7.0×10^{21}	8.4×10^{28}	8.0×10^{27}	1.7×10^{32}
		(0.1381)	(0.0016)	(0.0069)	(16×10^{-5})	0.60	1.5×10^{22}	1.8×10^{29}	1.8×10^{28}	3.8×10^{32}
^{132}Ba	$\beta^+\beta^+$	0.1103	0.0007	0.0013	3×10^{-5}	0.77				
		(0.0332)	(0.0006)	(0.0011)	(3×10^{-5})	0.60				
	β^+EC	0.2226	0.0009	0.0027	4×10^{-5}	0.77				
		(0.0678)	(0.0007)	(0.0022)	(5×10^{-5})	0.60				
	ECEC	0.2207	0.0009	0.0027	4×10^{-5}	0.77	5.9×10^{24}	2.4×10^{38}		
		(0.0664)	(0.0007)	(0.0022)	(5×10^{-5})	0.60	1.6×10^{25}	6.5×10^{38}		
^{136}Ce	$\beta^+\beta^+$	0.0922	0.0014	0.0008	5×10^{-5}	0.83	6.8×10^{31}			
		(0.0305)	(0.0013)	(0.0006)	(6×10^{-5})	0.60	2.5×10^{32}			
	β^+EC	0.1934	0.0023	0.0016	13×10^{-5}	0.83	1.0×10^{24}	7.8×10^{30}		
		(0.1366)	(0.0022)	(0.0013)	(14×10^{-5})	0.60	3.7×10^{24}	2.9×10^{31}		
	ECEC	0.1844	0.0018	0.0015	10×10^{-5}	0.83	1.6×10^{22}	2.3×10^{29}	7.7×10^{28}	7.3×10^{33}
		(0.0609)	(0.0017)	(0.0012)	(11×10^{-5})	0.60	5.9×10^{22}	8.5×10^{29}	2.8×10^{29}	2.7×10^{34}

The calculated half-lives of $2\nu\beta^+$/EC decays are presented in Tables VII and VIII. The matrix elements of the processes involving electron capture can be calculated separately for an electron captured from the K shell and an electron from the L shell. The values of these matrix elements are often very close to each other and, to a reasonable approximation, the mean value of these matrix elements can be used to represent the β^+EC- and ECEC-type transitions. The matrix elements given in Tables VII and VIII are the mean values of the K-capture and L-capture matrix elements for the β^+EC mode and KK and KL matrix elements for the ECEC mode. The half-lives are again calculated by using the linear g_A model and a constant $g_A = 0.6$.

The positron-emitting double-β^+ and EC decays have so far eluded experimental detection, thus making it difficult to evaluate the success of our predictions. However, the study of β^--type decays gave a general insight of the quality of the predictions therein, and a similar level of accuracy is to be expected for the positron-emitting transitions.

One should also note that the NMEs of the different modes of positron decay are quite in the same order of magnitude, but the half-lives differ largely. It is thus not the matrix element but the phase-space integral which determines the order of the half-lives of the different modes. Of the positron-decay modes, the ECEC channel to the ground state appears to be the fastest in every investigated process. The β^+EC mode is not far behind in some cases. These modes in the ground-state decay of ^{106}Cd, ^{112}Sn, and ^{130}Ba, with predicted half-lives of the order of 10^{21} years, seem favorable for experimental investigation in the future.

TABLE IX. The computed half-lives of double-positron decay of ^{106}Cd compared with Ref. [18].

Mode	$t_{1/2}$(y)		
	Ref. [18]	$g_A = 0.52$	$g_A = 0.60$
$\beta^+\beta^+$ gs $\rightarrow$ gs	1.8×10^{27}	8.1×10^{26}	4.6×10^{26}
β^+EC gs $\rightarrow$ gs	4.4×10^{22}	1.5×10^{22}	8.5×10^{21}
β^+EC gs $\rightarrow 0^+_2$	5.8×10^{26}	2.2×10^{26}	1.3×10^{26}
ECEC gs $\rightarrow$ gs	5.5×10^{21}	2.5×10^{21}	1.4×10^{21}
ECEC gs $\rightarrow 0^+_2$	3.4×10^{23}	2.0×10^{23}	1.1×10^{23}

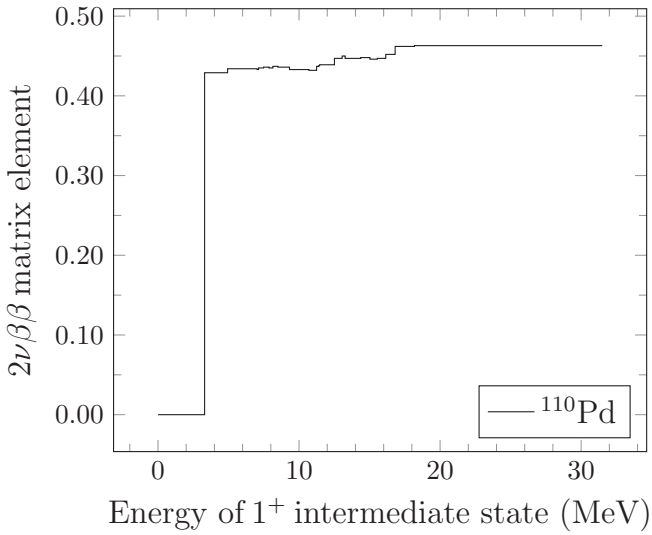

FIG. 10. The accumulation of the $2\nu\beta^-\beta^-$ matrix element of ^{110}Pd decay to ground state. The SSDH works to a reasonable approximation.

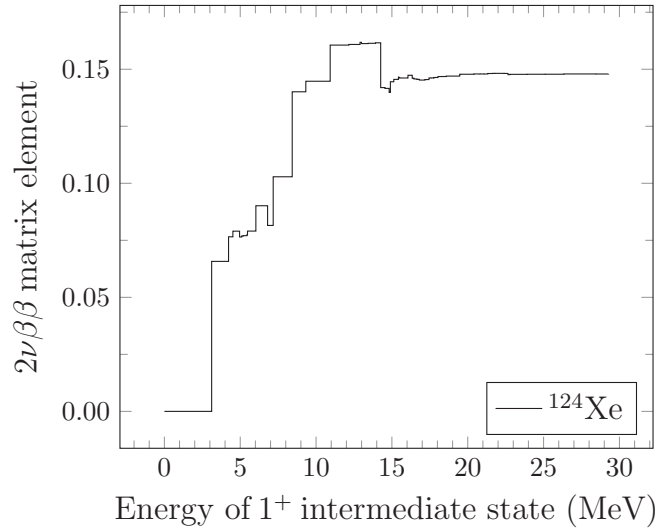

FIG. 12. The accumulation of the $2\nu\beta^+\beta^+$ matrix element of ^{124}Xe decay to ground state. The SSDH, in this case, is not realized.

The $2\nu\beta^-$ decays of the nuclei ^{104}Ru, ^{110}Pd, and ^{124}Sn were calculated recently in Ref. [30]. One should notice that in Ref. [30] only the lower limits of the half-lives were given due to difficulties in determining the model parameters accurately. No systematic analysis of the β-decay transitions was performed there such that it could help in determining the $2\nu\beta^-$ half-lives more accurately. The lower limits calculated in Ref. [30] are in good agreement with our present results. Our calculated values for both the linear and constant g_A appear to systematically lie roughly one order of magnitude above the lower limits. The approach to fitting the model parameters in Ref. [30] was based on a choice of values for g_A that were less quenched than the values found in the present work by varying both g_A and g_{pp}.

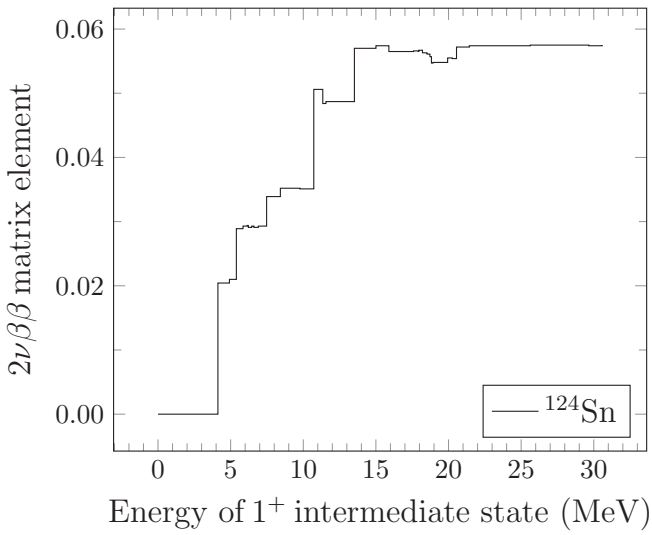

FIG. 11. The accumulation of the $2\nu\beta^-\beta^-$ matrix element of ^{124}Sn decay to ground state. The SSDH, in this case, is not realized.

The double-β decays of ^{106}Cd were previously treated theoretically in Refs. [18,19]. In Ref. [18] the $2\nu\beta^+$/EC and in Ref. [19] the $0\nu\beta^+$/EC decays were computed. A comparison of our present work with the 2001 results of Ref. [18] is made in Table IX. Our linear g_A model as well as the constant $g_A = 0.6$ predict the transitions of ^{106}Cd systematically slightly faster than the method used in Ref. [18]. The orders of magnitude are generally the same. As there is no experimental data available for double-positron decay modes, it is difficult to evaluate the results further.

The case of ^{124}Xe $2\nu\beta^+$/EC and $0\nu\beta^+$/EC decays was treated in Ref. [22]. The decay half-lives of the $2\nu\beta^+$/EC mode have a wide range of variation in Ref. [22] since the fixing of the model parameters in that work was rather loose due to the lack in experimental input and in systematic study of the model parameters. Contrariwise, in the present work the obtained systematics help pin down the calculated half-lives more accurately. Comparing our calculated $2\nu\beta^+$/EC half-lives with the corresponding ones of Fig. 2 of Ref. [22] we notice that our results with both the linear and constant g_A predict the half-lives to be longer than those in Ref. [22], especially for the decay to the ground state of ^{124}Te where the present predictions do not quite fit the range of variation in Ref. [22]. In decays to higher excited states the calculated half-life intervals of Ref. [22] are so wide that they contain our present results, which still always lie toward the longer end of the half-life interval. In Ref. [22] the values of the axial-vector coupling constant were varied within $g_A = 1.00$–1.25, which is a range that is higher than the effective value of g_A given by our present analysis. The values of g_{pp} in Ref. [22] were taken to be $g_{pp} = 0.80$–0.90, corresponding to the range of g_A. This range of g_{pp} fits our analysis of Fig. 3 but here we find that the effective value of g_A for these isobars is required to be quenched below 1.00 by the systematics of single-β decay. Considering the quite different adopted values of g_A, the differences in the present work and Ref. [22] seem reasonable.

TABLE X. The main contributions to the $2\nu\beta\beta$ matrix elements from intermediate states. The first column names the decaying nucleus, and the following columns list the QRPA energies of the intermediate 1^+ states and their contribution to the NME in descending order from the largest contribution.

Nucleus	Main contributions										
	Mode	E(MeV)	Contr.	E(MeV)	Contr.	E(MeV)	Contr.	E(MeV)	Contr.	E(MeV)	Contr.
^{100}Mo	$\beta^-\beta^-$	3.26	0.618								
^{104}Ru	$\beta^-\beta^-$	3.22	0.615	16.34	0.011						
^{110}Pd	$\beta^-\beta^-$	3.30	0.429								
^{114}Cd	$\beta^-\beta^-$	3.30	0.342								
^{116}Cd	$\beta^-\beta^-$	3.21	0.188	12.61	0.011						
^{122}Sn	$\beta^-\beta^-$	3.91	0.030	9.33	0.019	5.19	0.009	7.17	0.006		
^{124}Sn	$\beta^-\beta^-$	4.12	0.020	10.72	0.015	5.39	0.008	13.52	0.008	7.48	0.005
^{128}Te	$\beta^-\beta^-$	3.48	0.030	8.42	0.018	8.95	0.017	4.58	0.012	10.72	0.010
^{130}Te	$\beta^-\beta^-$	3.48	0.032	7.94	0.027	15.23	−0.024	8.78	0.019	15.50	0.015
^{134}Xe	$\beta^-\beta^-$	8.89	0.028	3.45	0.027	7.44	0.020	15.31	−0.017	4.61	0.012
^{136}Xe (a)	$\beta^-\beta^-$	7.99	0.023	4.87	0.016	11.03	0.015	16.09	−0.012	12.57	−0.008
^{136}Xe (b)	$\beta^-\beta^-$	7.99	0.020	11.03	0.013	4.87	0.011	16.09	−0.011	12.57	−0.007
^{102}Pd	$\beta^+\beta^+$	3.68	0.729								
	β^+EC	3.68	1.513								
	ECEC	3.68	1.457								
^{106}Cd	$\beta^+\beta^+$	3.33	0.934								
	β^+EC	3.33	2.203								
	ECEC	3.33	1.869								
^{108}Cd	$\beta^+\beta^+$	2.99	0.805	15.47	0.013						
	β^+EC	2.99	1.631	15.47	0.026						
	ECEC	2.99	1.609	15.47	0.026						
^{112}Sn	$\beta^+\beta^+$	3.21	0.784								
	β^+EC	3.21	1.717								
	ECEC	3.21	1.568								
^{120}Te	$\beta^+\beta^+$	3.57	0.067	9.09	0.022	6.85	−0.022	6.56	0.020	17.17	0.012
	β^+EC	3.57	0.141	9.09	0.044	6.85	−0.044	6.56	0.041	17.17	0.023
	ECEC	3.57	0.133	9.09	0.044	6.85	−0.044	6.56	0.040	17.17	0.021
^{124}Xe	$\beta^+\beta^+$	3.12	0.066	8.43	0.037	7.17	0.021	14.26	−0.020	10.93	0.016
	β^+EC	3.12	0.140	8.43	0.075	7.17	0.043	14.26	−0.039	10.93	0.032
	ECEC	3.12	0.132	8.43	0.075	7.17	0.043	14.26	−0.039	10.93	0.032
^{126}Xe	$\beta^+\beta^+$	3.31	0.054	8.59	0.040	7.33	0.018	4.43	0.014	10.74	0.012
	β^+EC	3.31	0.110	8.59	0.080	7.33	0.035	4.43	0.027	10.74	0.025
	ECEC	3.31	0.108	8.59	0.080	7.33	0.035	4.43	0.027	10.74	0.025
^{130}Ba	$\beta^+\beta^+$	3.42	0.069	8.84	0.060	4.53	0.018	14.85	−0.014	15.78	0.014
	β^+EC	3.42	0.156	8.84	0.122	4.53	0.037	14.85	−0.029	15.78	0.028
	ECEC	3.42	0.138	8.84	0.121	4.53	0.036	14.85	−0.029	15.78	0.028
^{132}Ba	$\beta^+\beta^+$	8.99	0.034	3.50	0.033	7.92	0.018	4.64	0.012	10.23	0.007
	β^+EC	3.50	0.068	8.99	0.067	7.92	0.036	4.64	0.025	10.23	0.025
	ECEC	8.99	0.067	3.50	0.066	7.92	0.035	4.64	0.024	10.23	0.015
^{136}Ce	$\beta^+\beta^+$	9.13	0.031	3.37	0.030	7.45	0.018	7.19	−0.008	6.42	0.006
	β^+EC	3.37	0.068	9.13	0.061	7.45	0.036	7.19	−0.016	4.53	0.013
	ECEC	9.13	0.062	3.37	0.061	7.45	0.036	7.19	−0.016	6.42	0.012

The single-state dominance hypothesis (SSDH) was discussed systematically in Refs. [56,57]. In the present study the following nuclear systems seem to satisfy the criteria of SSDH: ^{100}Mo, ^{104}Ru, ^{110}Pd, ^{114}Cd, and ^{116}Cd of the β^--type processes and ^{102}Pd, ^{106}Cd, ^{108}Cd, and ^{112}Sn of the β^+/EC-type processes. The realization of the SSDH appears to be dependent on the mass number A. The contributions from higher intermediate states start to dominate after $A = 116$, giving the transition more strength than with the first contribution only. Typical accumulation of the NMEs is depicted in Figs. 10–12 for the $\beta^-\beta^-$ decay of ^{110}Pd and ^{124}Sn and the $\beta^+\beta^+$ decay of ^{124}Xe respectively. One can see in Fig. 10 that the running sum of the ^{110}Pd NME gains its final magnitude almost solely from the first intermediate state and the behavior after the first state is nearly constant. For the ^{124}Sn and ^{124}Xe decay processes the graphs are more lively and saturate to a constant final magnitude after the intermediate state at roughly 14 MeV. Although this is in the typical energy range of the Gamow-Teller giant resonance state, in these cases the centroid of the involved GTGR lies somewhat higher in

energy. Some minor contributions are still attributed to the GTGR centroid and states nearby. The largest contributions from single intermediate states to the NMEs are listed in Table X. In all cases the contributions stem mainly from the first intermediate state and only few other states. Only in a few cases does the largest contribution come from some other state than the first 1^+ intermediate state.

IV. CONCLUSIONS

In this work we have scanned experimental data on Gamow-Teller β^- and β^+/EC decay rates (comparative half-lives, i.e., $\log ft$ values) in triplets of nuclear isobars in the mass region $A = 100$–136. We found 24 triplets where an odd-odd nucleus appears between two even-even nuclei and the connecting β-decay transitions have measured $\log ft$ values. The decay amplitudes associated to the mentioned decays can also be calculated, in this case by the proton-neutron QRPA. In the present analysis we have used the geometric mean of the two β-decay rates since, owing to the characteristic behavior of the pnQRPA-computed β^- and β^+/EC decay amplitudes, that quantity is almost independent of the value of the $g_{\rm pp}$ parameter of the pnQRPA. The experimental geometric means can be reproduced for each triplet separately by varying the value of the axial-vector coupling constant $g_{\rm A}$. Our study predicts a rough piecewise linear increase in the value of $g_{\rm A}$ as a function of the mass number A. We have used this A dependence of $g_{\rm A}$ to predict two-neutrino double-β decay half-lives, both for the $2\nu\beta^-$ and $2\nu\beta^+$/EC transitions, in altogether 21 isobaric triplets. Decays to both the ground state and lowest few excited states have been considered and a comparison has been made between results for the linear $g_{\rm A}$ and an average constant value of $g_{\rm A} = 0.6$.

The linear model for $g_{\rm A}$ was found to be quite accurate in describing the ground-state-to-ground-state single-β decays with $g_{\rm pp} = 0.7$. This value of the particle-particle parameter was then adopted for the examination of the double-β decays. The calculated half-lives for $\beta^-\beta^-$ decays were in decent agreement with experimental data in cases where such data was available although better accuracy was obtained by using the constant value of $g_{\rm A} = 0.6$. This seems to support the conclusions of Refs. [37,38] that the single- and double-β decays follow a different trend in terms of variation of $g_{\rm A}$.

For the half-lives of the remaining $\beta^-\beta^-$ processes as well as the positron-emitting double-β^+/EC decays with no present experimental data, our study produced predictions that can be expected to be not more than an order of magnitude off the true values. The most attractive processes to probe experimentally in the future seem to be ground-state-to-ground-state decays of ^{110}Pd ($\beta^-\beta^-$), ^{106}Cd (ECEC), and ^{112}Sn (ECEC) with predicted half-lives of 2.2×10^{20}, $(1.4 - 2.5) \times 10^{21}$, and $(7.4 - 9.6) \times 10^{21}$ years respectively.

ACKNOWLEDGMENTS

This work has been partially supported by the Academy of Finland under the Finnish Center of Excellence Program 2012–2017 (Nuclear and Accelerator Based Program at JYFL).

[1] J. Suhonen and O. Civitarese, Phys. Rep. **300**, 123 (1998).
[2] F. T. Avignone III, S. R. Elliott, and J. Engel, Rev. Mod. Phys. **80**, 481 (2008).
[3] J. Vergados, H. Ejiri, and F. Šimkovic, Rep. Prog. Phys. **75**, 106301 (2012).
[4] J. Suhonen and O. Civitarese, J. Phys. G: Nucl. Part. Phys. **39**, 085105 (2012).
[5] J. Toivanen and J. Suhonen, Phys. Rev. Lett. **75**, 410 (1995).
[6] C. M. Raduta and A. A. Raduta, Phys. Rev. C **82**, 068501 (2010).
[7] E. Caurier, G. Martinez-Pinedo, F. Nowacki, A. Poves, and A. Zuker, Rev. Mod. Phys. **77**, 427 (2005).
[8] J. Barea and F. Iachello, Phys. Rev. C **79**, 044301 (2009).
[9] T. R. Rodríguez and G. Martínez-Pinedo, Phys. Rev. Lett. **105**, 252503 (2010).
[10] P. K. Rath, R. Chandra, K. Chaturvedi, P. K. Raina, and J. G. Hirsch, Phys. Rev. C **82**, 064310 (2010).
[11] J. Suhonen and O. Civitarese, J. Phys. G: Nucl. Part. Phys. **39**, 124005 (2012).
[12] A. S. Barabash, Phys. Rev. C **81**, 035501 (2010).
[13] M. Doi and T. Kotani, Prog. Theor. Phys. **87**, 1207 (1992).
[14] J. Suhonen, Phys. Rev. C **48**, 574 (1993).
[15] M. Hirsch, K. Muto, T. Oda, and H. Klapdor-Kleingrothaus, Z. Phys. A **347**, 151 (1994).
[16] M. Aunola and J. Suhonen, Nucl. Phys. A **602**, 133 (1996).
[17] J. Toivanen and J. Suhonen, Phys. Rev. C **55**, 2314 (1997).
[18] J. Suhonen and O. Civitarese, Phys. Lett. B **497**, 221 (2001).
[19] J. Suhonen, Phys. Lett. B **701**, 490 (2011).
[20] J. Suhonen, Phys. Rev. C **86**, 024301 (2012).
[21] J. Suhonen, Phys. Rev. C **87**, 034318 (2013).
[22] J. Suhonen, J. Phys. G: Nucl. Part. Phys. **40**, 075102 (2013).
[23] B. H. Wildenthal, M. S. Curtin, and B. A. Brown, Phys. Rev. C **28**, 1343 (1983).
[24] G. Martínez-Pinedo, A. Poves, E. Caurier, and A. P. Zuker, Phys. Rev. C **53**, R2602 (1996).
[25] A. Juodagalvis and D. J. Dean, Phys. Rev. C **72**, 024306 (2005).
[26] E. Caurier, F. Nowacki, and A. Poves, Phys. Lett. B **711**, 62 (2012).
[27] P. Vogel and M. R. Zirnbauer, Phys. Rev. Lett. **57**, 3148 (1986).
[28] O. Civitarese, A. Faessler, and T. Tomoda, Phys. Lett. B **194**, 11 (1987).
[29] J. Suhonen, Phys. Lett. B **607**, 87 (2005).
[30] J. Suhonen, Nucl. Phys. A **864**, 63 (2011).
[31] V. A. Rodin, A. Faessler, F. Šimkovic, and P. Vogel, Nucl. Phys. A **766**, 107 (2006).
[32] M. Kortelainen and J. Suhonen, Phys. Rev. C **75**, 051303(R) (2007).
[33] M. Kortelainen and J. Suhonen, Phys. Rev. C **76**, 024315 (2007).
[34] J. Suhonen and M. Kortelainen, Int. J. Mod. Phys. E **17**, 1 (2008).
[35] A. Faessler, G. L. Fogli, E. Lisi, V. Rodin, A. M. Rotunno, and F. Šimkovic, J. Phys. G **35**, 075104 (2008).
[36] J. Barea, J. Kotila, and F. Iachello, Phys. Rev. C **87**, 014315 (2013).
[37] J. Suhonen and O. Civitarese, Phys. Lett. B **725**, 153 (2013).
[38] J. Suhonen and O. Civitarese, Nucl. Phys. A **924**, 1 (2014).

[39] N. Yoshida and F. Iachello, Prog. Theor. Exp. Phys. **2013**, 043D01 (2013).
[40] H. Ejiri, N. Soukouti, and J. Suhonen, Phys. Lett. B **729**, 27 (2014).
[41] D. S. Delion and J. Suhonen, Eur. Phys. Lett. **107**, 52001 (2014).
[42] J. Suhonen, *From Nucleons to Nucleus: Concepts of Microscopic Nuclear Theory* (Springer, Berlin, 2007).
[43] M. Doi, T. Kotani, and E. Takasugi, Prog. Theor. Phys. Suppl. **83**, 1 (1985).
[44] J. Suhonen, Nucl. Phys. A **563**, 205 (1993).
[45] O. Civitarese and J. Suhonen, Nucl. Phys. A **575**, 251 (1994).
[46] D. S. Delion and J. Suhonen, Phys. Rev. C **67**, 034301 (2003).
[47] A. Bohr and B. R. Mottelson, *Nuclear Structure* (Benjamin, New York, 1969), Vol. 1.
[48] J. Suhonen, T. Taigel, and A. Faessler, Nucl. Phys. A **486**, 91 (1988).
[49] A. H. Wapstra and G. Audi, Nucl. Phys. A **432**, 1 (1985).
[50] G. Audi, F. G. Kondev, M. Wang, B. Pfeiffer, X. Sun, J. Blachot, and M. MacCormick, Chin. Phys. C **36**, 1157 (2012).
[51] J. Suhonen and O. Civitarese, Nucl. Phys. A **584**, 449 (1995).
[52] National Nuclear Data Center, Chart of Nuclides [http://www.nndc.bnl.gov/chart/].
[53] V. S. Shirley *et al.*, *Table of Isotopes, Seventh Edition*, 7th ed. (John Wiley & Sons, New York, 1978).
[54] A. S. Barabash, AIP Conf. Proc. **1572**, 11 (2013).
[55] V. I. Tretyak and Y. G. Zdesenko, At. Data Nucl. Data Tables **80**, 83 (2002).
[56] O. Civitarese and J. Suhonen, Phys. Rev. C **58**, 1535 (1998).
[57] O. Civitarese and J. Suhonen, Nucl. Phys. A **653**, 321 (1999).